bioRxiv preprint doi: https://doi.org/10.1101/2024.07.30.605839; this version posted November 25, 2024. The copyright holder for this preprint (which was not certified by peer review) is the author/funder, who has granted bioRxiv a license to display the preprint in perpetuity. It is made available under aCC-BY-ND 4.0 International license.

HIV-1 Vif disrupts phosphatase feedback regulation at the kinetochore, leading to a pronounced pseudo-metaphase arrest

Dhaval Ghone[1, 2, 6], Edward L. Evans III[1, 3, 5, 6, 8], Madison Bandini[1, 3, 5], Kaelyn G. Stephenson[1], Nathan M. Sherer[1, 4, 5, *], Aussie Suzuki[1, 4, 7, *]

1. McArdle Laboratory for Cancer Research, Department of Oncology, University of Wisconsin-Madison, Madison, Wisconsin, USA
2. Biophysics Graduate Program, University of Wisconsin-Madison, Madison, Wisconsin, USA
3. Cancer Biology Graduate Program, University of Wisconsin-Madison, Madison, Wisconsin, USA
4. Carbone Comprehensive Cancer Center, University of Wisconsin-Madison, Madison, Wisconsin, USA
5. Institute for Molecular Virology, University of Wisconsin-Madison, Madison, Wisconsin 53706, USA
6. These authors contributed equally
7. Lead contact
8. Present address: Laboratory for Optical and Computational Instrumentation, University of Wisconsin-Madison, Madison, Wisconsin, 53705, USA

* Corresponding authors: Aussie Suzuki (aussie.suzuki@wisc.edu) and Nathan Sherer (nsherer@wisc.edu)

bioRxiv preprint doi: https://doi.org/10.1101/2024.07.30.605839; this version posted November 25, 2024. The copyright holder for this preprint (which was not certified by peer review) is the author/funder, who has granted bioRxiv a license to display the preprint in perpetuity. It is made available under aCC-BY-ND 4.0 International license.

Abstract

Virion Infectivity Factor (Vif) of the Human Immunodeficiency Virus type 1 (HIV-1) targets and degrades cellular APOBEC3 proteins, key regulators of intrinsic and innate antiretroviral immune responses, thereby facilitating HIV-1 infection. While Vif's role in degrading APOBEC3G is well-studied, Vif is also known to cause cell cycle arrest, but the detailed nature of Vif's effects on the cell cycle has yet to be delineated. In this study, we employed high-temporal single-cell live imaging and super-resolution microscopy to monitor individual cells during Vif-induced cell cycle arrest. Our findings reveal that Vif does not affect the G2/M boundary as previously thought. Instead, Vif triggers a unique and robust pseudo-metaphase arrest, distinct from the mild prometaphase arrest induced by Vpr. During this arrest, chromosomes align properly and form the metaphase plate, but later lose alignment, resulting in polar chromosomes. Notably, Vif, unlike Vpr, significantly reduces the levels of both Protein Phosphatase 1 (PP1) and 2A (PP2A) at kinetochores, which regulate chromosome-microtubule interactions. These results unveil a novel role for Vif in kinetochore regulation that governs the spatial organization of chromosomes during mitosis.

bioRxiv preprint doi: https://doi.org/10.1101/2024.07.30.605839; this version posted November 25, 2024. The copyright holder for this preprint (which was not certified by peer review) is the author/funder, who has granted bioRxiv a license to display the preprint in perpetuity. It is made available under aCC-BY-ND 4.0 International license.

Introduction

The human immunodeficiency virus type 1 (HIV-1) weakens the immune system by depleting CD4+ T cells, eventually causing the Acquired Immunodeficiency Syndrome (AIDS) (Deeks et al, 2015; Swanstrom & Coffin, 2012). As a result, HIV-1 infected individuals have an increased susceptibility to specific cancers and other health complications (Cohen et al, 2016; Grulich et al, 2007; Hernández-Ramírez et al, 2017; Parkin, 2006). After HIV-1 enters a host cell, its RNA genome undergoes reverse transcription to form double-stranded DNA, followed by integration of the DNA provirus into the host's genome. Using the host's transcriptional machinery, HIV-1 transcribes its genome into spliced, partially spliced and completely unspliced viral mRNAs, facilitating viral gene expression and infectious virion production (Jouvenet et al, 2009; Nguyen & Hildreth, 2000; Ono & Freed, 2001). While the mechanisms underlying CD4+ T cell depletion during HIV-1 infection remain an active area of research, evidence suggests that both direct cytopathic effects of HIV-1 and chronic hyperactivation of the immune system contribute significantly. These processes drive apoptosis and induce pyroptosis in CD4+ T cells, leading to their progressive loss (Doitsh & Greene, 2016; Vidya Vijayan *et al*, 2017).

HIV-1 encodes four accessory viral proteins (Vif, Vpr, Vpu, and Nef) that are nonessential for virus replication in some ex vivo cell culture systems (Gabuzda et al, 1992) but play crucial immunomodulatory roles in vivo (Malim & Emerman, 2008). The primary role of Vif (Virion

bioRxiv preprint doi: https://doi.org/10.1101/2024.07.30.605839; this version posted November 25, 2024. The copyright holder for this preprint (which was not certified by peer review) is the author/funder, who has granted bioRxiv a license to display the preprint in perpetuity. It is made available under aCC-BY-ND 4.0 International license.

Infectivity Factor) is to facilitate the proteasomal degradation of APOBEC3 (A3) family of cytidine deaminases (e.g., A3F, A3G, and A3H). A3 proteins introduce deleterious mutations into the HIV-1 genome by deaminating cytosine residues in the viral single-stranded DNA during reverse-transcription, converting them to uracil (Chiu & Greene, 2009; Okada & Iwatani, 2016). Vif orchestrates A3 protein degradation by recruiting an E3 ubiquitin ligase complex (Conticello et al, 2003; Marin et al, 2003; Sheehy et al, 2003; Stopak et al, 2003; Yu et al, 2003). This degradation prevents A3 proteins from being incorporated into budding viral particles, ensuring that the progeny virions remain infectious.

Independently of its primary role of A3 protein degradation (DeHart et al, 2008; Du et al, 2019; Zhao et al, 2015), several studies have shown Vif to induce cell cycle arrest and cell death in CD4+ T cells and several other cell types (DeHart et al., 2008; Du et al., 2019; Greenwood et al, 2016; Marelli et al, 2020; Nagata et al, 2020; Sakai et al, 2006; Salamango et al, 2019; Zhao et al., 2015). However, the molecular mechanisms that underpin these effects remain unclear. A prior study indicated that p53, a tumor suppressor, is required for Vif-induced G2/M cell cycle arrest (Izumi et al, 2010). Several recent studies suggest that Vif's cell cycle arrest activity is due to the loss of B56 proteins that are regulatory subunits of protein phosphatase 2A (PP2A) (DeHart et al., 2008; Du et al., 2019; Greenwood et al., 2016; Marelli et al., 2020; Nagata et al., 2020; Salamango et al., 2019; Salamango et al, 2020; Zhao et al., 2015). The PP2A-B56

bioRxiv preprint doi: https://doi.org/10.1101/2024.07.30.605839; this version posted November 25, 2024. The copyright holder for this preprint (which was not certified by peer review) is the author/funder, who has granted bioRxiv a license to display the preprint in perpetuity. It is made available under aCC-BY-ND 4.0 International license.

complex is a serine-threonine protein phosphatase that participates in various key G2 and mitotic processes (Lee et al, 2017; Schuhmacher et al, 2019). Additionally, earlier research has demonstrated that Vif can lead to reductions in Cyclin F (Augustine et al, 2017), a non-canonical cyclin critical for late S- and G2-phase progression (Clijsters et al, 2019; Enrico et al, 2021), or affect both Cdk1 and Cyclin B1, which are essential for the transition into and out of mitosis (Sakai et al, 2011).

These prior studies have predominantly employed flow cytometry-based techniques to measure cell cycle phase population densities. However, flow cytometry has limitations in its ability to differentiate between late S, G2, and M phases, because it categorizes cell cycle phases solely based on relative DNA content. Accordingly, in this study we prioritized high-temporal single-cell live imaging that would allow us to directly observe the disruptions of cell cycle triggered by Vif expression. We demonstrate that Vif induces a highly unique and robust pseudo-metaphase arrest, irrespective of cell line tested or p53 status. Additionally, we found that Vpr unexpectedly induces a distinct mitotic delay, clearly different from the pseudo-metaphase arrest caused by Vif. Vif, but not Vpr, disrupts the localizations of PP2A-B56 at the kinetochores during prometaphase, leading to a slight yet significant delay in the alignment of chromosome at metaphase. This disruption results in reduced localization of the Astrin-SKAP-PP1 complex at the kinetochores, causing improper kinetochore-microtubule binding affinity due

bioRxiv preprint doi: https://doi.org/10.1101/2024.07.30.605839; this version posted November 25, 2024. The copyright holder for this preprint (which was not certified by peer review) is the author/funder, who has granted bioRxiv a license to display the preprint in perpetuity. It is made available under aCC-BY-ND 4.0 International license.

to increased phosphorylation of the microtubule binding protein at kinetochores. These effects yield unbalanced forces between sister chromatids, resulting in misaligned chromosomes and abnormal chromosomal movements in association with spindle microtubules. These insights provide a deeper understanding of Vif's impact on the regulation of the host cell cycle, a conserved feature of Vif that may have potential relevance to HIV-1 pathogenesis in vivo.

bioRxiv preprint doi: https://doi.org/10.1101/2024.07.30.605839; this version posted November 25, 2024. The copyright holder for this preprint (which was not certified by peer review) is the author/funder, who has granted bioRxiv a license to display the preprint in perpetuity. It is made available under aCC-BY-ND 4.0 International license.

Results

Vif and Vpr induce distinct forms of mitotic arrest

Previous research demonstrated that both Vif and Vpr expression causes cell cycle arrest and cytotoxicity in CD4+ T cells and as well as many cancer cell lines (Augustine *et al.*, 2017; Emerman, 1996; Evans *et al*, 2018; Nagata *et al.*, 2020; Sakai *et al.*, 2011; Sakai *et al.*, 2006; Salamango *et al.*, 2019; Salamango *et al.*, 2020; Wang *et al*, 2011; Wang *et al*, 2008). To investigate the nature of the cell cycle arrest induced by Vif, we employed high-temporal live cell imaging using the triple negative breast cancer Cal51 cell line. This cell line was chosen for several reasons; it has been engineered for precise cell cycle tracking through CRISPR-Cas9-mediated endogenous tagging of Histone H2B with mScarlet, allowing visualization of DNA, and Tubulin with mNeonGreen, to enable monitoring the microtubule cytoskeleton (Scribano et al, 2021). This approach minimizes the confounding effects of exogenous overexpression of fluorescently labeled Histone and Tubulin proteins on cell cycle progression (**Fig 1A**). Moreover, Cal51 cells are well-suited for long-term live cell imaging assays due to their adherent growth properties, which facilitate extended single-cell monitoring. They also exhibit a stable, near-diploid karyotype and retain wild-type p53 expression, making them an ideal model for cell cycle research (Lynch et al, 2022). For these experiments, we infected cells with the NL4-3 strain HIV-1 reporter viruses expressing either Vif (“Vif”), Vpr (“Vpr”), a combination of both (“Vif+Vpr”), or

bioRxiv preprint doi: https://doi.org/10.1101/2024.07.30.605839; this version posted November 25, 2024. The copyright holder for this preprint (which was not certified by peer review) is the author/funder, who has granted bioRxiv a license to display the preprint in perpetuity. It is made available under aCC-BY-ND 4.0 International license.

a lack of both ("Control") (**Fig S1A**) (Evans *et al.*, 2018). Note that the NL4-3 strain encodes all known HIV-1 proteins and serves as a well-established model for studying various aspects of HIV-1 biology (Mustafa & Robinson, 1993). These reporter viruses contain cyan fluorescent protein (CFP), allowing us to identify infected cells under fluorescence microscopy. To focus our study on the effects of these proteins on the cell cycle, the reporter viruses do not express the viral Env and Nef proteins, which are known to exhibit cytotoxicity (Elder, 2002; Emerman, 1996; Evans *et al.*, 2018).

We then assessed the mitotic duration defined as the time between nuclear envelope breakdown (NEBD) and anaphase onset in CFP-positive cells using video microscopy. Vif-expressing Cal51 cells demonstrated a prolonged mitosis of ~16 hours, in contrast to only 30 min in Control cells (**Fig 1B and Movies S1-2**). Great majority of Vif-expressing cells eventually succumbed to apoptotic cell death or exhibited mitotic slippage, wherein the cell exited mitosis without completing chromosome segregation (**Fig 1C and S1B**).

Vpr has been known to induce G2/M arrest in a variety of cell types, as evidenced by flowcytometry (Bartz *et al*, 1996; Elder, 2002; Emerman, 1996; Hall *et al*, 2024; He *et al*, 1995; Jowett *et al*, 1995; Sakai *et al.*, 2006). We next examined the differences in G2/M arrests induced by Vif and Vpr. While we expected Vpr to induce G2 phase arrest due to its abilities to cause DNA damage, our live-cell imaging revealed that Vpr-expressing cells also experienced a

bioRxiv preprint doi: https://doi.org/10.1101/2024.07.30.605839; this version posted November 25, 2024. The copyright holder for this preprint (which was not certified by peer review) is the author/funder, who has granted bioRxiv a license to display the preprint in perpetuity. It is made available under aCC-BY-ND 4.0 International license.

prolonged mitosis of ~1.7 hours, which is significantly shorter than in Vif-expressing cells (**Fig 1A-B**). Interestingly, Vif+Vpr-expressing cells exhibited a prolonged mitosis lasting ~21.7 hours, indicating that Vif plays a dominant role in mitotic arrest when both proteins are present. Supporting this, the majority of Vif-expressing or Vif+Vpr-expressing mitotic cells underwent apoptotic cell death, whereas Vpr-expressing mitotic cells either completed division or experienced mitotic slippage. In summary, although both Vif and Vpr can induce a prolonged mitosis, Vif causes significantly more severe mitotic arrest, leading to cell death.

To pinpoint the specific sub-stage of mitosis affected by Vif expression, we closely assessed chromosome alignment during metaphase. Notably, most Vif-expressing Cal51 cells successfully achieved metaphase chromosome alignment (metaphase plate) similar to the control cells, but with a slight delay, reaching it approximately 1.5 hours post-NEBD compared to the control's ~30 minutes. (**Fig 2A-C**). However, this alignment was unstable and deteriorated over time in Vif-expressing cells. Mitotic arrest induced by common mitotic inhibitors is seen in prometaphase before achieving the metaphase plate (Choi et al, 2011). However, the mitotic arrest caused by Vif was distinctive because cells were able to complete prometaphase but then gradually lost proper chromosome spatial organization at the metaphase plate over time. Accordingly, we termed this block “pseudo-metaphase arrest”. Consistent with our findings in Cal51 cells, other commonly used cell lines for cell cycle studies, such as HeLa and MDA-MB-

bioRxiv preprint doi: https://doi.org/10.1101/2024.07.30.605839; this version posted November 25, 2024. The copyright holder for this preprint (which was not certified by peer review) is the author/funder, who has granted bioRxiv a license to display the preprint in perpetuity. It is made available under aCC-BY-ND 4.0 International license.

231, also demonstrated significant mitotic arrest (approximately 12 hours for both) following Vif expression, which subsequently led to either apoptotic cell death or mitotic slippage (**Fig S1C-E and S2A-C**). Similar to Cal51, the majority of these Vif-expressing cells were able to establish a metaphase plate early but were unable to enter anaphase (**Fig S1F-G and S2D-E**). Consistent with these results, Vif-expressing HeLa cells exhibited a markedly higher mitotic index compared to Control cells at 72 hours post-infection in fixed immunofluorescence (IF) (**Fig S1H**). In conclusion, Vif triggers a marked pseudo-metaphase arrest in a range of cell lines. Most of these arrested cells experienced either apoptotic cell death or mitotic slippage, suggesting a conserved underlying mechanism.

Solo Vif expression is sufficient to trigger a robust pseudo-metaphase arrest

To determine if Vif expression alone is sufficient to induce a robust pseudo-metaphase arrest in the absence of other viral factors, we next engineered HeLa cells to conditionally express codon optimized Vif (CO-Vif) under the control of a doxycycline-inducible promoter (Das et al, 2016). As a control, we employed the same system but with mNeonGreen expression instead of Vif. Control cells displayed mNeonGreen signals approximately 10 hours post-doxycycline induction. In line with these expression kinetics, cells expressing CO-Vif almost invariably exhibited pseudo-metaphase arrest roughly 10 hours post-induction; with cells

bioRxiv preprint doi: https://doi.org/10.1101/2024.07.30.605839; this version posted November 25, 2024. The copyright holder for this preprint (which was not certified by peer review) is the author/funder, who has granted bioRxiv a license to display the preprint in perpetuity. It is made available under aCC-BY-ND 4.0 International license.

arrested for ~15h in contrast to Control cells that proceeded through mitosis in ~1 hour (**Fig 2D-E and Movies S3-4**). While Control cells continued to propagate, those expressing Vif did not, with Vif expression alone confirmed as sufficient to trigger prolonged pseudo-metaphase arrest and apoptotic cell death (**Fig 2F-G**).

Vif accelerates G2 progression with no effect on the G1 or S phases

We next asked if Vif altered other stages of the cell cycle in addition to mitosis. To this end, we developed a novel method that allowed us to accurately distinguish between G1, S, and G2 phases in individual Cal51 reporter cells during live cell imaging based on tracking changes to the intensity of Histone H2B-mScarlet over time (see **Methods**). This method offers the advantage of allowing us to measure temporal changes of the DNA content at single cell resolution with high accuracy. Briefly, during S phase, H2B-mScarlet signals increased steadily, eventually plateauing and remaining constant throughout the G2 phase. **Fig 3A** presents example images and an intensity profile covering the period from the end of one mitosis to the beginning of the next in a Control Cal51 cell. Using this method, we observed no significant differences in the durations of either G1 or S phases in both Control or Vif-expressing cells. However, Vif-expressing cells exhibited a slight yet statistically significant reduction in G2 phase duration compared to Control cells (**Fig 3B-C and S3A**). Consistent to Cal51 cells, Vif expression

bioRxiv preprint doi: https://doi.org/10.1101/2024.07.30.605839; this version posted November 25, 2024. The copyright holder for this preprint (which was not certified by peer review) is the author/funder, who has granted bioRxiv a license to display the preprint in perpetuity. It is made available under aCC-BY-ND 4.0 International license.

also did not significantly impact the duration of interphase in two additional cell lines, RPE1 and MDA-MB-231 cells (**Fig. S3B).** In summary, these findings demonstrated that Vif expression induces pseudo-metaphase arrest without notably affecting the overall duration of interphase (the cumulative time of G1, S, and G2 phases).

Vif Induces Pseudo-Metaphase Arrest Independently of p53

A previous study indicated that Vif-induced cell cycle arrest is due to tumor suppressor p53 (Izumi et al., 2010), which is well established to trigger G2 cell cycle arrest in response to DNA damage (St Clair et al, 2004; Stark & Taylor, 2006; Taylor & Stark, 2001). Considering that we had already observed Vif inducing pseudo-metaphase arrest in cell lines with functionally inactivated p53, such as HeLa (Evans et al., 2018; Wang et al., 2011) and MDA-MB-231 (Olivier et al, 2002) (**Fig S1C-D and S2A-B**), we further investigated the potential p53-dependency by assessing Vif's effects in p53 null knockout (p53 KO) RPE1 (Mardin et al, 2015) or HCT116 cell lines (**Fig 3D-G**). Both wild-type (p53 +/+) and p53 KO RPE1 and HCT116 cells demonstrated significant pseudo-metaphase arrest in response to viral Vif expression. Specifically, RPE1 wild-type cells were arrested for >10 hours, RPE1 p53 KO cells for ~25 hours, and both HCT116 wild-type and p53 KO cells for >6 hours. In contrast, cells infected with the Vif-negative Control virus showed no delay in mitosis (~30 min for both cell lines) (**Fig 3D-E and S3D-E**). All cell lines,

bioRxiv preprint doi: https://doi.org/10.1101/2024.07.30.605839; this version posted November 25, 2024. The copyright holder for this preprint (which was not certified by peer review) is the author/funder, who has granted bioRxiv a license to display the preprint in perpetuity. It is made available under aCC-BY-ND 4.0 International license.

235 regardless of p53 status, managed to establish a chromosome metaphase plate in the presence
236 of Vif expression (**Fig 3F-G and S3F-G**). However, most Vif-expressing cells exhibited apoptotic
237 cell death or mitotic slippage (**Fig S3C and S3H**).
238
239 **Vif-induced pseudo-metaphase arrest disrupts spatial organization of chromosomes and**
240 **spindle poles**
241 To further characterize the mitotic defects caused by Vif expression, we carefully
242 assessed Vif's effects on chromosome alignment at the metaphase plate. To this end, we
243 employed super-resolution microscopy and stained for CENP-C, microtubules, and DNA (see
244 **Methods**). CENP-C is a marker for kinetochores, the platform for microtubule attachment on
245 mitotic chromosomes. Our findings revealed that ~100% of Vif-expressing mitotic cells exhibited
246 misaligned chromosomes, with the great majority of these misaligned chromosomes
247 concentrated at spindle poles as polar chromosomes (**Fig 4A-B, S4A, and Movies S5-6**).
248 We next explored the dynamics of chromosome spatial organization in Vif-expressing
249 cells by using live cell imaging. To do this, we first quantified the proportion of cells exhibiting
250 polar chromosomes at any time point during metaphase/pseudo-metaphase for all four of our
251 cell systems (HeLa, RPE1, MDA-MB-231, and Cal51 cells). Consistent with our fixed-cell
252 analysis, we observed ~100% of Vif-expressing cells exhibiting misaligned polar chromosomes

bioRxiv preprint doi: https://doi.org/10.1101/2024.07.30.605839; this version posted November 25, 2024. The copyright holder for this preprint (which was not certified by peer review) is the author/funder, who has granted bioRxiv a license to display the preprint in perpetuity. It is made available under aCC-BY-ND 4.0 International license.

253 at some time point during the prolonged mitosis, in contrast to Control cells in which misaligned
254 chromosomes were only rarely observed (**Fig S4B**). To define the dynamic nature of
255 chromosome movements, we segmented cells into two compartments, polar and equatorial, and
256 then measured the Histone H2B-mScarlet signals within each of these compartments in Cal51
257 cells over time (**Fig 4C**). Vif-expressing cells exhibited an initial decrease in the frequency of
258 polar chromosomes shortly after NEBD, but this frequency increased significantly during the
259 extended pseudo-metaphase; with pronounced polar chromosomes comprising ~50% of the
260 total DNA. Notably, these misaligned chromosomes continuously oscillated between the poles
261 and the metaphase plate, as shown in **Fig 4D**.

262 Consistent with abnormal chromosome dynamics, ~25% of HeLa cells expressing Vif
263 exhibited multi-polar spindles (>2 poles) at 72h post-infection based on fixed cell analysis (**Fig**
264 **S4C**). To corroborate these findings, we used high-temporal live cell imaging to track and
265 quantify spindle poles using mNeonGreen-Tubulin in Cal51 cells. We observed that ~80% of
266 cells expressing Vif demonstrated multi-polarity at some time point during the extended mitosis.
267 Moreover, the number of spindle poles varied dramatically in arrested cells, ranging from a
268 monopole to as many as five poles (**Fig 4E and S4D**).

269 The integrity of spindle poles is crucial for maintaining the position of the metaphase
270 plate during mitotic progression, so that the length of microtubules making up the mitotic spindle

bioRxiv preprint doi: https://doi.org/10.1101/2024.07.30.605839; this version posted November 25, 2024. The copyright holder for this preprint (which was not certified by peer review) is the author/funder, who has granted bioRxiv a license to display the preprint in perpetuity. It is made available under aCC-BY-ND 4.0 International license.

is tightly regulated and typically remains stable until anaphase onset. Interestingly, we found that mitotic spindles in Vif-expressing cells were significantly stretched (~18 μm in length) as compared to Control cells (~12 μm) (**Fig 4F and S4E**). Moreover, although mitotic spindles are typically stationary, we observed spindles in Vif-expressing cells to exhibit dynamic spinning. To define these observations quantitatively, we measured the average angle swept by individual mitotic spindles over time in the presence or absence of Vif expression, observing a greater than 15-fold increase in the angle covered by spindles in Vif-expressing cells as compared to Control cells (**Fig 4G and S4F**). In summary, Vif induces dynamic movements in both chromosomes and spindle poles during extended pseudo-metaphase, resulting in severely misaligned polar chromosomes.

Vif, but not Vpr, disrupts the proper localization of PP2A-B56 at the kinetochores

Microtubule assembly at the kinetochore is regulated by an intricate network of kinase and phosphatases (Saurin, 2018). PP2A-B56 is recruited to kinetochores during prometaphase, where it plays a crucial role in microtubule assembly and the proper alignment of chromosomes (Foley & Kapoor, 2013; Foley *et al*, 2011). Previous studies demonstrated that Vif can significantly degrade B56 proteins, as shown by western blots (Greenwood *et al.*, 2016; Marelli *et al.*, 2020; Nagata *et al.*, 2020). Therefore, we investigated whether Vif-expressing mitotic cells

bioRxiv preprint doi: https://doi.org/10.1101/2024.07.30.605839; this version posted November 25, 2024. The copyright holder for this preprint (which was not certified by peer review) is the author/funder, who has granted bioRxiv a license to display the preprint in perpetuity. It is made available under aCC-BY-ND 4.0 International license.

had diminished B56 at kinetochores. To address this, we performed quantitative immunofluorescence (qIF) using specific antibodies against B56 and CENP-C (as a kinetochore marker) in Control, Vif-expressing, and Vpr-expressing cells. We found that B56 signals at kinetochores, regardless of aligned (equatorial) or unaligned (polar) chromosomes, were significantly reduced in Vif-expressing cells compared to Control and Vpr-expressing cells (**Fig 5A-C**). To determine whether Vif-expressing cells remained free of additional, non-kinetochore-bound pools of B56, we performed qIF in nocodazole treated cells. It has been demonstrated that nocodazole, microtubule depolymerizer, can enhance B56 kinetochore localization (Foley *et al.*, 2011). As expected, Control cells showed further recruitment of B56 to kinetochores upon nocodazole treatment, whereas Vif-expressing cells did not (**Fig 5A and 5C**). These results suggest that Vif-mediated degradation of B56 is sufficient to significantly reduce B56 levels at kinetochores during prometaphase, while Vpr has no effect on B56 levels at kinetochores. To further validate these results, we performed qIF on Polo-like Kinase 1 (Plk1). Plk1 is a key cell cycle regulator with critical roles at kinetochores in proper mitotic progression (Colicino & Hehnly, 2018). It is known that Plk1 levels at kinetochores are regulated by PP2A-B56, and depletion of B56 causes increased levels of Plk1 at kinetochores, leading to improper microtubule attachments (Foley *et al.*, 2011). As expected, Plk1 levels at kinetochores were significantly dropped in metaphase as compared to prometaphase in Control cells (**Fig 5D-E**). In Vif-

bioRxiv preprint doi: https://doi.org/10.1101/2024.07.30.605839; this version posted November 25, 2024. The copyright holder for this preprint (which was not certified by peer review) is the author/funder, who has granted bioRxiv a license to display the preprint in perpetuity. It is made available under aCC-BY-ND 4.0 International license.

307 expressing cells, while Plk1 levels at kinetochores in equatorial chromosomes were lower than
308 those on polar chromosomes, Vif-expressing cells showed a global increase in Plk1 levels at
309 kinetochores. More specifically, Plk1 levels at polar chromosomes in Vif-expressing cells were
310 significantly higher than in Control prometaphase, and levels at aligned equatorial chromosomes
311 were also significantly higher than in Control metaphase. In summary, Vif, but not Vpr,
312 significantly diminishes PP2A-B56 levels at kinetochores, resulting in a delay of chromosome
313 alignments.

314

315 **Vif impairs stable and balanced kinetochore microtubule attachments**

316 We demonstrated that Vif-expressing cells exhibited abnormal dynamic chromosome
317 movements (**Fig 4D-G**). Kinetochore-microtubule bindings are stabilized by both PP2-B56 and
318 PP1 at kinetochores through an interplay and feedback mechanism (Saurin, 2018; Vallardi *et al*,
319 2017). Consequently, we hypothesized that the reduction of PP2A-B56 by Vif impaired the
320 regulation PP1 phosphatase activities at kinetochores. To test this hypothesis, we quantified the
321 levels of the Astrin-SKAP complex (hereinafter referred to as 'Astrin') at kinetochores by qIF in
322 HeLa cells in the presence or absence of Vif expression. Astrin stabilizes kinetochore-
323 microtubule attachments by recruiting PP1, which dephosphorylates Hec1, a microtubule
324 binding protein at kinetochores, thereby promoting Hec1 binding to microtubules (Cheeseman

bioRxiv preprint doi: https://doi.org/10.1101/2024.07.30.605839; this version posted November 25, 2024. The copyright holder for this preprint (which was not certified by peer review) is the author/funder, who has granted bioRxiv a license to display the preprint in perpetuity. It is made available under aCC-BY-ND 4.0 International license.

et al, 2006; Conti *et al*, 2019; Dunsch *et al*, 2011; Manning *et al*, 2010; Schmidt *et al*, 2010; Zhang *et al*, 2015). As expected, Astrin signals at kinetochores significantly increased at metaphase compared to prometaphase in Control cells (**Fig 6A-B**). In contrast, Astrin levels at kinetochores on aligned chromosomes (equatorial) in Vif-expressing cells were approximately 50% of control, and Astrin levels on polar chromosomes largely undetectable (**Fig 6A-B**). We confirmed that levels of CENP-C, which is a core-structural kinetochore protein, did not change between Control and Vif-expressing cells, indicating that the reduction of Astrin in Vif-expressing cells was not due to compromised kinetochore integrity (**Fig 6A-B**).

Generating uniform pulling force across sister kinetochores is essential for maintaining chromosome alignment at the cell equator during metaphase. While control cells showed equal Astrin recruitment at sister kinetochores, consistent with balanced forces (**Fig 6C)**, Vif-expressing cells showed significant differences in Astrin levels between sister kinetochores despite CENP-C levels remaining consistent (**Fig 6B-C)**.

The N-terminal domain of Hec1 has multiple phosphorylation sites, and dephosphorylation specifically by PP1 is critical for stabilizing its binding to microtubules (DeLuca *et al*, 2011). To directly validate the reduced activity of PP1 at kinetochores in Vif-expressing cells, we performed qIF using a phospho-Hec1 S55 antibody (pS55). As expected, phosphorylation levels pS55 were high in Control prometaphase and significantly reduced in

bioRxiv preprint doi: https://doi.org/10.1101/2024.07.30.605839; this version posted November 25, 2024. The copyright holder for this preprint (which was not certified by peer review) is the author/funder, who has granted bioRxiv a license to display the preprint in perpetuity. It is made available under aCC-BY-ND 4.0 International license.

metaphase (**Fig 6D-E**). In contrast, pS55 levels remained significantly high at aligned chromosomes (equatorial) in Vif-expressing cells compared to aligned metaphase chromosomes in Control cells (**Fig 6D-E**). Similarly, unaligned chromosomes (Polar) maintained pS55 levels similar to those in Control prometaphase. We confirmed that Hec1 levels at kinetochores were the same in both Vif-expressing and Control cells (**Fig 6G-H**). These results demonstrate that PP1 activity at kinetochores is weaker in Vif-expressing cells compared to Control cells. In agreement with the unbalanced Astrin recruitment at sister kinetochores in Vif-expressing cells, pS55 levels between sister kinetochores were also significantly unbalanced in Vif-expressing cells compared to Control cells (**Fig 6F**). In summary, Vif disrupts the proper assembly of the Astrin-PP1 complex at kinetochores, resulting in the retention of high phosphorylation Hec1 levels. This leads to weakened and uneven forces between sister kinetochores, likely contributing to dynamic chromosome movements.

Limitations of the study

To study the spatiotemporal regulation of Vif and the effects of its expression levels at the single-cell level, we aimed to visualize Vif's trafficking during the cell cycle. We discovered that C-terminal fusion of tags, such as 3xHA or mCherry, abolishes Vif's ability to induce pseudo-metaphase arrest (**Fig S5A-E**). In this study, we elucidate the mechanisms underlying Vif-

bioRxiv preprint doi: https://doi.org/10.1101/2024.07.30.605839; this version posted November 25, 2024. The copyright holder for this preprint (which was not certified by peer review) is the author/funder, who has granted bioRxiv a license to display the preprint in perpetuity. It is made available under aCC-BY-ND 4.0 International license.

induced pseudo-metaphase arrest by utilizing cancer cell lines and a non-transformed normal cell line. While performing similar high-temporal resolution long-term imaging on well-established host cell types for HIV-1 (primary CD4+ T cells, lymphocytes, dendritic cells, or macrophages) poses significant technical challenges, future studies are required to investigate these cell types. Such investigations will help determine whether Vif can contribute to the suppression of the host immune system by effectively induce robust pseudo-metaphase arrest, ultimately leading to cell death.

Discussion

The specific processes by which HIV-1 causes loss of CD4+ T cells are numerous and include activation of innate immune sensors (Doitsh & Greene, 2016), Envelope-driven cell fusion/syncytiation (Nardacci et al, 2015), and induction of cell cycle arrest followed by programmed cell death mediated by viral gene products that include Vif and Vpr (Muthumani et al, 2005). Vif has recently been shown to induce cell cycle arrest in conjunction with its downregulation of PP2A-B56 subunits (Marelli et al., 2020; Nagata et al., 2020; Salamango et al., 2019). However, the specific nature of this arrest was not previously examined at the level of single cells and had been assumed to occur during G2 based on flow cytometric assays. In

bioRxiv preprint doi: https://doi.org/10.1101/2024.07.30.605839; this version posted November 25, 2024. The copyright holder for this preprint (which was not certified by peer review) is the author/funder, who has granted bioRxiv a license to display the preprint in perpetuity. It is made available under aCC-BY-ND 4.0 International license.

our study, we discovered that expression of Vif actually reduces the duration of G2 (**Fig 3B**) and instead triggers a robust pseudo-metaphase arrest, confirmed in a broad range of cell lines, and with cells typically succumbing to apoptotic cell death after extended pseudo-metaphase (**Fig 1C, 1H, S1E, S2C**). We also demonstrate that, contrary to a prior study (Izumi et al., 2010), Vif-induced pseudo-metaphase arrest occurs independently of p53 status (**Fig 3D-F and S3D-F**).

Further, we demonstrate that Vif specifically disrupts the kinetochore functions, impairing proper mitotic progression (**Fig. 6A-B)**. Normally, after NEBD, microtubules efficiently capture kinetochores during prometaphase through the interplay of PP1 and PP2A-B56 phosphatase activities (Sivakumar & Gorbsky, 2017; Smith *et al*, 2019; Vallardi *et al.*, 2017). PP2A-B56 is recruited to kinetochores in prometaphase, reducing Plk1 activity to facilitate kinetochore-microtubule assembly and promoting recruitment of PP1 by multiple adaptors. A major PP1 adaptor for kinetochore recruitment is the Astrin-SKAP complex whose recruitment requires proper microtubule end-on attachment (Conti *et al.*, 2019; Friese *et al*, 2016; McVey *et al*, 2021). In Vif-expressing cells, Vif significantly reduces the level of PP2A-B56 at kinetochore in prometaphase, likely due to its role in B56 degradation. This reduction leads to a slower establishment of metaphase plate (**Fig 7**). The significant loss of PP2A-B56 at kinetochores impairs the feedback control necessary for stabilizing microtubule binding. As a result, there is a significantly lower and uneven recruitment of Astrin-SKAP-PP1 complex to kinetochores,

bioRxiv preprint doi: https://doi.org/10.1101/2024.07.30.605839; this version posted November 25, 2024. The copyright holder for this preprint (which was not certified by peer review) is the author/funder, who has granted bioRxiv a license to display the preprint in perpetuity. It is made available under aCC-BY-ND 4.0 International license.

causing uneven pulling forces between sister chromatids that result in some chromosomes being prematurely pulled towards spindle poles prior to satisfying the mitotic checkpoint (**Fig 7D, Step 1**). Upon approaching the spindle poles, Aurora A, another key kinase that regulates mitotic error correction, phosphorylates the MTBDs of Ndc80/Hec1 and destabilizes kinetochore-microtubule attachment (**Fig 7D, Step 2**) (Anna *et al*, 2015; Barr & Gergely, 2007; Chmátal *et al*, 2015; DeLuca, 2017; DeLuca *et al.*, 2011; Kettenbach *et al*, 2011). This destabilization of the kinetochore-microtubule attachment could explain why polar chromosomes in Vif-expressing cells lose Astrin signals at kinetochores (**Fig 6A-B**). Polar chromosomes are then transported back to the equator by polar-ejection forces (**Fig 7D, Step 3**) (Poser et al, 2019; Wandke et al, 2012). The repetition of this cycle accounts for the observed abnormal dynamics of chromosome movements in Vif-expressing cells.

Acknowledgement

We would like to thank YuHi Hara, Takanori Tsuchiya, Yokogawa Corporation, Nikon, and Tokai Hit for critical equipment and technical support. We also would like to thank Dr. James Bruce for the critical suggestions and experimental support and Ms. Ainslie Homan for support in data analysis. Part of this work is supported by the University of Wisconsin-Madison Office of the Vice

bioRxiv preprint doi: https://doi.org/10.1101/2024.07.30.605839; this version posted November 25, 2024. The copyright holder for this preprint (which was not certified by peer review) is the author/funder, who has granted bioRxiv a license to display the preprint in perpetuity. It is made available under aCC-BY-ND 4.0 International license.

Chancellor for Research with funding from the Wisconsin Alumni Research Foundation, start-up funding from University of Wisconsin-Madison SMPH, UW Carbone Cancer Center, and McArdle Laboratory for Cancer Research, and NIH grant R35GM147525 and U54AI170660 (to A.S.) and U54AI170660, R01AI110221, and P01CA022443 (to N.S.).

Author contribution

E.L.E. III initiated the project, identified Vif-induced metaphase arrest, and generated key viral reagents and NL4-3 strain HIV-1 reporter vectors. D.G. conducted the bulk of the follow-up precision imaging experiments and analyses, with assistance from M.B., K.G.S., N.S., and A.S.. A.S. and N.S. conceptualized, supervised and funded the project. D.G. and A.S. prepared the initial manuscript draft, with assistance from N.S., E.L.E. III, and M.B. All authors reviewed and contributed to the manuscript's refinement.

Competing Financial Interests

The authors declare no further conflict of interests.

Methods

Cell Culture

bioRxiv preprint doi: https://doi.org/10.1101/2024.07.30.605839; this version posted November 25, 2024. The copyright holder for this preprint (which was not certified by peer review) is the author/funder, who has granted bioRxiv a license to display the preprint in perpetuity. It is made available under aCC-BY-ND 4.0 International license.

Human HeLa, RPE1, Cal51, and MDA-MB-231 cells were originally obtained from the American Type Culture Collection (ATCC, Manassas, VA, USA). RPE1 p53 KO, HCT116 p53 KO, RPE1 (H2B-RFP), MDA-MB-231 (H2B-mCherry), and Cal51 (Tubulin-mNeonGreen and H2B-mScarlet were endogenously tagged by CRISPR-Cas9) cells were originally obtained from Dr. Jan Korbel, Dr. Yue Xiong (UNC), Dr. Mark Burkard, and Dr. Beth Weaver, respectively. H2B-GFP expressing HeLa cells and conditional CO-Vif-expressing HeLa cells using a pCEP4 vector (Thermo) containing the TRE and Tet promotor with codon-optimized Vif or mNeonGreen were generated in this study. HeLa, MDA-MB-231, HCT116, RPE1 and Cal51 were grown in DMEM high glucose (Cytiva Hyclone; SH 30243.01) or DMEM/F12 (Cytiva Hyclone; SH 3026101) supplemented with 1% penicillin-streptomycin, 1% L-glutamine, and 10% fetal bovine serum under 5% CO_2 at 37ºC in an incubator.

Live cell imaging

RPE1, Cal51, HeLa, and MDA-MB-231 cells were plated on 4-chamber 35mm glass bottom dishes at least one day prior to imaging (4 chamber with #1.5 glass, Cellvis). In a subset of experiments, cells were stained using sirDNA (Cytoskeleton, 150 nM) for 2 hours prior to imaging to visualize chromosomal DNA. For conditionally Vif-expressing cells, doxycycline (1 µg/ml, Sigma) was supplemented prior to imaging. High temporal resolution live-cell imaging was

bioRxiv preprint doi: https://doi.org/10.1101/2024.07.30.605839; this version posted November 25, 2024. The copyright holder for this preprint (which was not certified by peer review) is the author/funder, who has granted bioRxiv a license to display the preprint in perpetuity. It is made available under aCC-BY-ND 4.0 International license.

performed using a Nikon Ti2 inverted microscope equipped with a Hamamatsu Fusion camera, spectra-X LED light source (Lumencor), Shiraito PureBox (TokaiHit), and a Plan Apo 20x objective (NA = 0.75) controlled by Nikon Elements software. Cells were recorded at 37°C with 5% CO2 in a stage-top incubator using the feedback control function to accurately maintain temperature of growth medium (Tokai Hit, STX model). Images were recorded for 48-120 hours at 6-12 min intervals with three to four z-stack images acquired at steps of 1.5~2 μm for each time point.

Fixed high- and super-resolution imaging

HeLa cells infected “Control” (Vif-negative) and Vif-containing viruses were fixed by 4% PFA (Sigma) at 72 hours post-infection. Cells were then permeabilized by 0.5% NP40 (Sigma) and incubated with 0.5% BSA (Sigma). Following primary and secondary antibodies were used; CENP-C (MBL), Tubulin (Sigma), GFP (Thermo), B56-alpha (BD Biosciences), Plk1 (Santa Cruz), Astrin (Sigma), Hec1/9G3 (Abcam), Hec1 pS55 (GeneTex), anti-mouse IgG Alexa 488 (min X, JacksonImmuno research), anti-guinea pig IgG Rhodamine Red X (min X, Jackson immune research), anti-guinea pig IgG Alexa 647 (min X, JacksonImmuno research), anti-rabbit IgG Alexa-488 (JacksonImmuno research) and anti-rabbit Alexa 647 (min X, Jackson immune research). Stained samples were imaged both CSU W1 spinning disc confocal and CSU W1

bioRxiv preprint doi: https://doi.org/10.1101/2024.07.30.605839; this version posted November 25, 2024. The copyright holder for this preprint (which was not certified by peer review) is the author/funder, who has granted bioRxiv a license to display the preprint in perpetuity. It is made available under aCC-BY-ND 4.0 International license.

SoRa super-resolution (Yokogawa) confocal microscope (Loi et al, 2023). These spinning disc confocal units were equipped with a Nikon Ti2 inverted microscope with a Hamamatsu Fusion camera, Shiraito PureBox (TokaiHit), and a TIRF SR 100x objective (NA = 1.49). The microscope system was controlled by Nikon Elements software (Nikon). Figure 3B images were generated using Imaris software (Andor).

Image analysis

Image analysis was performed using Nikon Elements software (Nikon) or Metamorph (Molecular Devices). Mitotic stages and errors were determined by nuclear staining. The mitotic duration was defined as the time from nuclear envelope breakdown (NEBD) to anaphase onset. Timepoints of formation and loss of metaphase plate were documented. CFP signals were used as a marker for infected cells. Tubulin-mNeonGreen was used for quantifying numbers of spindle poles and monitoring their dynamics. Spindle pole distance was measured when spindle poles were maximally stretched in high-temporal live cell images using Nikon Elements.

Cell cycle phase analysis

To track cell cycle progression, H2B signals were measured over time using Nikon NIS Elements on time lapse images of Cal51 cells. Signal intensities were measured manually and the local

bioRxiv preprint doi: https://doi.org/10.1101/2024.07.30.605839; this version posted November 25, 2024. The copyright holder for this preprint (which was not certified by peer review) is the author/funder, who has granted bioRxiv a license to display the preprint in perpetuity. It is made available under aCC-BY-ND 4.0 International license.

487 background correction method (Loi *et al.*, 2023; Suzuki *et al*, 2015) was applied to accurately
488 quantify chromatin signal intensity. Signals were collected in this manner at 18-30 min intervals.
489 The duration of each cell cycle stage was determined by analyzing changes in the H2B-mScarlet
490 signal over time.
491
492 **Polar chromosome quantification**
493 Cell segmentation and measurements of chromosome distribution were performed using the
494 Nikon NIS Elements program. First, the region-of-interest (ROI) tool was used to select
495 chromosomes located at each pole or at the equator. Corrected signal intensity was calculated
496 using a local background correction method (Suzuki *et al.*, 2015). Measurements were made for
497 every 6 minutes for the first 2 hours after NEBD, and for every ~1.5 hours subsequently. For
498 each time point, the percentage of polar chromosomes was calculated using the following
499 formula: (Corrected intensity of Pole1+Pole2)*100/(Corrected intensity of
500 Pole1+Pole2+Equator).
501
502 **Spindle rotation measurements**
503 Measurements of spindle rotation were performed using the Nikon Elements program's Manual
504 Measurement tool. Cells were observed after NEBD and the free angle tool was used to measure

bioRxiv preprint doi: https://doi.org/10.1101/2024.07.30.605839; this version posted November 25, 2024. The copyright holder for this preprint (which was not certified by peer review) is the author/funder, who has granted bioRxiv a license to display the preprint in perpetuity. It is made available under aCC-BY-ND 4.0 International license.

the absolute value of the spindle rotation angle traced from using either the spindle pole or the equatorial chromosomes as a reference. For control cells, measurements were made for each consecutive frame from the first frame where a spindle appeared until the first frame at the onset of anaphase. For Vif-expressing cells measurements were made for frames whenever a visually significant angle was traced. Data was exported to Excel. The Matplotlib library in Python was used to make polar plots, with time plotted as radius and angle traced plotted as theta.

Statistics

All experiments were independently repeated 2-3 times for mitotic duration measurements. p-values were calculated using one-way ANOVA and the two-tailed Student's t-test. p-values < 0.05 were considered significant. In the figures, p-values are denoted as * for ≤0.05, ** for ≤0.01, *** for ≤0.001 and **** for ≤0.0001.

Transduction and infection

For infections, growth media was replaced with viral supernatants carrying VSV-G-pseudo typed HIV-1 CFP reporter viruses (Vif-positive or Vif-negative) at a multiplicity of infection of ~1, with the viruses engineered and produced as previously described (Evans et al., 2018).

bioRxiv preprint doi: https://doi.org/10.1101/2024.07.30.605839; this version posted November 25, 2024. The copyright holder for this preprint (which was not certified by peer review) is the author/funder, who has granted bioRxiv a license to display the preprint in perpetuity. It is made available under aCC-BY-ND 4.0 International license.

References

Anna AY, Deretic J, Hoel CM, Hinman AW, Cimini D, Welburn JP, Maresca TJ (2015) Aurora A kinase contributes to a pole-based error correction pathway. *Current Biology* 25: 1842-1851

Augustine T, Chaudhary P, Gupta K, Islam S, Ghosh P, Santra MK, Mitra D (2017) Cyclin F/FBXO1 Interacts with HIV-1 Viral Infectivity Factor (Vif) and Restricts Progeny Virion Infectivity by Ubiquitination and Proteasomal Degradation of Vif Protein through SCFcyclin F E3 Ligase Machinery. *Journal of Biological Chemistry* 292: 5349-5363

Barr AR, Gergely F (2007) Aurora-A: the maker and breaker of spindle poles. *Journal of Cell Science* 120: 2987-2996

Bartz SR, Rogel ME, Emerman M (1996) Human immunodeficiency virus type 1 cell cycle control: Vpr is cytostatic and mediates G2 accumulation by a mechanism which differs from DNA damage checkpoint control. *J Virol* 70: 2324-2331

Cheeseman IM, Chappie JS, Wilson-Kubalek EM, Desai A (2006) The conserved KMN network constitutes the core microtubule-binding site of the kinetochore. *Cell* 127: 983-997

Chiu Y-L, Greene WC (2009) APOBEC3G: an intracellular centurion. *Philosophical Transactions of the Royal Society B: Biological Sciences* 364: 689-703

Chmátal L, Yang K, Schultz RM, Lampson MA (2015) Spatial regulation of kinetochore microtubule attachments by destabilization at spindle poles in meiosis I. *Current Biology* 25: 1835-1841

Choi HJ, Fukui M, Zhu BT (2011) Role of Cyclin B1/Cdc2 Up-Regulation in the Development of Mitotic Prometaphase Arrest in Human Breast Cancer Cells Treated with Nocodazole. *Plos One* 6

Clijsters L, Hoencamp C, Calis JJA, Marzio A, Handgraaf SM, Cuitino MC, Rosenberg BR, Leone G, Pagano M (2019) Cyclin F Controls Cell-Cycle Transcriptional Outputs by Directing the Degradation of the Three Activator E2Fs. *Molecular Cell* 74: 1264-1277.e1267

Cohen MS, Chen YQ, McCauley M, Gamble T, Hosseinipour MC, Kumarasamy N, Hakim JG, Kumwenda J, Grinsztejn B, Pilotto JHS *et al* (2016) Antiretroviral Therapy for the Prevention of HIV-1 Transmission. *New England Journal of Medicine* 375: 830-839

Colicino EG, Hehnly H (2018) Regulating a key mitotic regulator, polo-like kinase 1 (PLK1). *Cytoskeleton (Hoboken)* 75: 481-494

Conti D, Gul P, Islam A, Martín-Durán JM, Pickersgill RW, Draviam VM (2019) Kinetochores attached to microtubule-ends are stabilised by Astrin bound PP1 to ensure proper chromosome segregation. *eLife* 8: e49325

Conticello SG, Harris RS, Neuberger MS (2003) The Vif protein of HIV triggers degradation of the human antiretroviral DNA deaminase APOBEC3G. *Current Biology* 13: 2009-2013

Das AT, Tenenbaum L, Berkhout B (2016) Tet-On Systems For Doxycycline-inducible Gene Expression. *Curr Gene Ther* 16: 156-167

Deeks SG, Overbaugh J, Phillips A, Buchbinder S (2015) HIV infection. *Nature Reviews Disease Primers* 1

DeHart JL, Bosque A, Harris RS, Planelles V (2008) Human immunodeficiency virus type 1 Vif induces cell cycle delay via recruitment of the same E3 ubiquitin ligase complex that targets APOBEC3 proteins for degradation. *Journal of virology* 82: 9265-9272

DeLuca JG, 2017. Aurora A kinase function at kinetochores, Cold Spring Harbor Symposia on Quantitative Biology. Cold Spring

bioRxiv preprint doi: https://doi.org/10.1101/2024.07.30.605839; this version posted November 25, 2024. The copyright holder for this preprint (which was not certified by peer review) is the author/funder, who has granted bioRxiv a license to display the preprint in perpetuity. It is made available under aCC-BY-ND 4.0 International license.

Harbor Laboratory Press, pp. 91-99.

DeLuca KF, Lens SMA, DeLuca JG (2011) Temporal changes in Hec1 phosphorylation control kinetochore–microtubule attachment stability during mitosis. *Journal of Cell Science* 124: 622-634

Doitsh G, Greene WC (2016) Dissecting How CD4 T Cells Are Lost During HIV Infection. *Cell Host Microbe* 19: 280-291

Du J, Rui Y, Zheng W, Li P, Kang J, Zhao K, Sun T, Yu X-F (2019) Vif-CBFβ interaction is essential for Vif-induced cell cycle arrest. *Biochemical and biophysical research communications* 511: 910-915

Dunsch AK, Linnane E, Barr FA, Gruneberg U (2011) The astrin–kinastrin/SKAP complex localizes to microtubule plus ends and facilitates chromosome alignment. *Journal of Cell Biology* 192: 959-968

Elder RT (2002) HIV-1 VPR modulates cell cycle G2/M transition through an alternative cellular mechanism other than the classic mitotic checkpoints. *Frontiers in Bioscience* 7

Emerman M (1996) HIV-1, Vpr and the cell cycle. *Current Biology* 6: 1096-1103

Enrico TP, Stallaert W, Wick ET, Ngoi P, Wang X, Rubin SM, Brown NG, Purvis JE, Emanuele MJ (2021) Cyclin F drives proliferation through SCF-dependent degradation of the retinoblastoma-like tumor suppressor p130/RBL2. *eLife* 10

Evans EL, Becker JT, Fricke SL, Patel K, Sherer NM, Kirchhoff F (2018) HIV-1 Vif's Capacity To Manipulate the Cell Cycle Is Species Specific. *Journal of Virology* 92

Foley EA, Kapoor TM (2013) Microtubule attachment and spindle assembly checkpoint signalling at the kinetochore. *Nat Rev Mol Cell Bio* 14: 25-37

Foley EA, Maldonado M, Kapoor TM (2011) Formation of stable attachments between kinetochores and microtubules depends on the B56-PP2A phosphatase. *Nat Cell Biol* 13: 1265-U1216

Friese A, Faesen AC, Huis in 't Veld PJ, Fischböck J, Prumbaum D, Petrovic A, Raunser S, Herzog F, Musacchio A (2016) Molecular requirements for the inter-subunit interaction and kinetochore recruitment of SKAP and Astrin. *Nature Communications* 7: 11407

Gabuzda DH, Lawrence K, Langhoff E, Terwilliger E, Dorfman T, Haseltine WA, Sodroski J (1992) Role of Vif in Replication of Human-Immunodeficiency-Virus Type-1 in Cd4+ T Lymphocytes. *Journal of Virology* 66: 6489-6495

Greenwood EJD, Matheson NJ, Wals K, van den Boomen DJH, Antrobus R, Williamson JC, Lehner PJ (2016) Temporal proteomic analysis of HIV infection reveals remodelling of the host phosphoproteome by lentiviral Vif variants. *Elife* 5: e18296

Grulich AE, van Leeuwen MT, Falster MO, Vajdic CM (2007) Incidence of cancers in people with HIV/AIDS compared with immunosuppressed transplant recipients: a meta-analysis. *The Lancet* 370: 59-67

Hall R, Ahern LM, Yap MW, Tsai M-HC, Boucherit VC, Takaki T, Boulton SJ, Bishop KN (2024) HIV-1 Vpr causes separate cell cycle arrests in G2 and M that activate alternative DNA damage pathways. *bioRxiv*: 2024.2004. 2002.587683

He J, Choe S, Walker R, Di Marzio P, Morgan DO, Landau NR (1995) Human immunodeficiency virus type 1 viral protein R (Vpr) arrests cells in the G2 phase of the cell cycle by inhibiting p34cdc2 activity. *J Virol* 69: 6705-6711

Hernández-Ramírez RU, Shiels MS, Dubrow R, Engels EA (2017) Cancer risk in HIV-infected people in the USA from 1996 to 2012: a population-based, registry-linkage study. *The Lancet HIV* 4: e495-e504

Izumi T, Io K, Matsui M, Shirakawa K, Shinohara M, Nagai Y, Kawahara M, Kobayashi M, Kondoh H, Misawa N *et al* (2010) HIV-1 viral infectivity factor interacts with TP53 to induce G2 cell cycle arrest and positively regulate viral replication. *Proceedings*

bioRxiv preprint doi: https://doi.org/10.1101/2024.07.30.605839; this version posted November 25, 2024. The copyright holder for this preprint (which was not certified by peer review) is the author/funder, who has granted bioRxiv a license to display the preprint in perpetuity. It is made available under aCC-BY-ND 4.0 International license.

of the National Academy of Sciences 107: 20798-20803

Jouvenet N, Simon SM, Bieniasz PD (2009) Imaging the interaction of HIV-1 genomes and Gag during assembly of individual viral particles. *Proceedings of the National Academy of Sciences* 106: 19114-19119

Jowett JB, Planelles V, Poon B, Shah NP, Chen ML, Chen IS (1995) The human immunodeficiency virus type 1 vpr gene arrests infected T cells in the G2 + M phase of the cell cycle. *J Virol* 69: 6304-6313

Kettenbach AN, Schweppe DK, Faherty BK, Pechenick D, Pletnev AA, Gerber SA (2011) Quantitative Phosphoproteomics Identifies Substrates and Functional Modules of Aurora and Polo-Like Kinase Activities in Mitotic Cells. *Science Signaling* 4: rs5-rs5

Lee SJ, Rodriguez-Bravo V, Kim H, Datta S, Foley EA (2017) The PP2AB56 phosphatase promotes the association of Cdc20 with APC/C in mitosis. *Journal of cell science*

Loi J, Qu X, Suzuki A (2023) Semi-automated 3D fluorescence speckle analyzer (3D-Speckler) for microscope calibration and nanoscale measurement. *The Journal of cell biology* 222

Lynch AR, Arp NL, Zhou AS, Weaver BA, Burkard ME (2022) Quantifying chromosomal instability from intratumoral karyotype diversity using agent-based modeling and Bayesian inference. *Elife* 11: e69799

Malim MH, Emerman M (2008) HIV-1 accessory proteins—ensuring viral survival in a hostile environment. *Cell host & microbe* 3: 388-398

Manning AL, Bakhoum SF, Maffini S, Correia ‐ Melo C, Maiato H, Compton DA (2010) CLASP1, astrin and Kif2b form a molecular switch that regulates kinetochore ‐ microtubule dynamics to promote mitotic progression and fidelity. *The EMBO Journal* 29: 3531-3543-3543

Mardin BR, Drainas AP, Waszak SM, Weischenfeldt J, Isokane M, Stütz AM, Raeder B, Efthymiopoulos T, Buccitelli C, Segura-Wang M *et al* (2015) A cell-based model system links chromothripsis with hyperploidy. *Mol Syst Biol* 11

Marelli S, Williamson JC, Protasio AV, Naamati A, Greenwood EJD, Deane JE, Lehner PJ, Matheson NJ (2020) Antagonism of PP2A is an independent and conserved function of HIV-1 Vif and causes cell cycle arrest. *eLife* 9

Marin M, Rose KM, Kozak SL, Kabat D (2003) HIV-1 Vif protein binds the editing enzyme APOBEC3G and induces its degradation. *Nature Medicine* 9: 1398-1403

McVey SL, Cosby JK, Nannas NJ (2021) Aurora B Tension Sensing Mechanisms in the Kinetochore Ensure Accurate Chromosome Segregation. *Int J Mol Sci* 22

Mustafa F, Robinson HL (1993) Context-dependent role of human immunodeficiency virus type 1 auxiliary genes in the establishment of chronic virus producers. *J Virol* 67: 6909-6915

Muthumani K, Choo AY, Premkumar A, Hwang DS, Thieu KP, Desai BM, Weiner DB (2005) Human immunodeficiency virus type 1 (HIV-1) Vpr-regulated cell death: insights into mechanism. *Cell Death Differ* 12: 962-970

Nagata K, Shindo K, Matsui Y, Shirakawa K, Takaori-Kondo A (2020) Critical role of PP2A-B56 family protein degradation in HIV-1 Vif mediated G2 cell cycle arrest. *Biochemical and biophysical research communications* 527: 257-263

Nardacci R, Perfettini JL, Grieco L, Thieffry D, Kroemer G, Piacentini M (2015) Syncytial apoptosis signaling network induced by the HIV-1 envelope glycoprotein complex: an overview. *Cell Death Dis* 6

Nguyen DH, Hildreth JEK (2000) Evidence for Budding of Human Immunodeficiency Virus Type 1 Selectively from Glycolipid-

bioRxiv preprint doi: https://doi.org/10.1101/2024.07.30.605839; this version posted November 25, 2024. The copyright holder for this preprint (which was not certified by peer review) is the author/funder, who has granted bioRxiv a license to display the preprint in perpetuity. It is made available under aCC-BY-ND 4.0 International license.

Enriched Membrane Lipid Rafts. *Journal of Virology* 74: 3264-3272

Okada A, Iwatani Y (2016) APOBEC3G-Mediated G-to-A Hypermutation of the HIV-1 Genome: The Missing Link in Antiviral Molecular Mechanisms. *Frontiers in Microbiology* 7

Olivier M, Eeles R, Hollstein M, Khan MA, Harris CC, Hainaut P (2002) The IARC TP53 database: New online mutation analysis and recommendations to users. *Human Mutation* 19: 607-614

Ono A, Freed EO (2001) Plasma membrane rafts play a critical role in HIV-1 assembly and release. *Proceedings of the National Academy of Sciences* 98: 13925-13930

Parkin DM (2006) The global health burden of infection-associated cancers in the year 2002. *Int J Cancer* 118: 3030-3044

Poser E, Caous R, Gruneberg U, Barr FA (2019) Aurora A promotes chromosome congression by activating the condensin-dependent pool of KIF4A. *Journal of Cell Biology* 219

Sakai K, Barnitz RA, Chaigne-Delalande B, Bidère N, Lenardo MJ (2011) Human Immunodeficiency Virus Type 1 Vif causes dysfunction of Cdk1 and CyclinB1: implications for cell cycle arrest. *Virology Journal* 8

Sakai K, Dimas J, Lenardo MJ (2006) The Vif and Vpr accessory proteins independently cause HIV-1-induced T cell cytopathicity and cell cycle arrest. *Proceedings of the National Academy of Sciences* 103: 3369-3374

Salamango DJ, Ikeda T, Moghadasi SA, Wang J, McCann JL, Serebrenik AA, Ebrahimi D, Jarvis MC, Brown WL, Harris RS (2019) HIV-1 Vif Triggers Cell Cycle Arrest by Degrading Cellular PPP2R5 Phospho-regulators. *Cell Reports* 29: 1057-1065.e1054

Salamango DJ, McCann JL, Demir Ö, Becker JT, Wang J, Lingappa JR, Temiz NA, Brown WL, Amaro RE, Harris RS *et al* (2020) Functional and Structural Insights into a Vif/PPP2R5 Complex Elucidated Using Patient HIV-1 Isolates and Computational Modeling. *Journal of Virology* 94

Saurin AT (2018) Kinase and Phosphatase Cross-Talk at the Kinetochore. *Front Cell Dev Biol* 6: 62

Schmidt JC, Kiyomitsu T, Hori T, Backer CB, Fukagawa T, Cheeseman IM (2010) Aurora B kinase controls the targeting of the Astrin–SKAP complex to bioriented kinetochores. *Journal of Cell Biology* 191: 269-280

Schuhmacher D, Sontag J-M, Sontag E (2019) Protein Phosphatase 2A: More Than a Passenger in the Regulation of Epithelial Cell–Cell Junctions. *Frontiers in Cell and Developmental Biology* 7

Scribano CM, Wan J, Esbona K, Tucker JB, Lasek A, Zhou AS, Zasadil LM, Molini R, Fitzgerald J, Lager AM *et al* (2021) Chromosomal instability sensitizes patient breast tumors to multipolar divisions induced by paclitaxel. *Science Translational Medicine* 13

Sheehy AM, Gaddis NC, Malim MH (2003) The antiretroviral enzyme APOBEC3G is degraded by the proteasome in response to HIV-1 Vif. *Nature Medicine* 9: 1404-1407

Sivakumar S, Gorbsky GJ (2017) Phosphatase-regulated recruitment of the spindle- and kinetochore-associated (Ska) complex to kinetochores. *Biol Open* 6: 1672-1679

Smith RJ, Cordeiro MH, Davey NE, Vallardi G, Ciliberto A, Gross F, Saurin AT (2019) PP1 and PP2A Use Opposite Phospho-dependencies to Control Distinct Processes at the Kinetochore. *Cell Rep* 28: 2206-2219 e2208

St Clair S, Giono L, Varmeh-Ziaie S, Resnick-Silverman L, Liu WJ, Padi A, Dastidar J, DaCosta A, Mattia M, Manfredi JJ (2004) DNA damage-induced downregulation of Cdc25C is mediated by p53 via two independent mechanisms:: One involves direct binding to the

bioRxiv preprint doi: https://doi.org/10.1101/2024.07.30.605839; this version posted November 25, 2024. The copyright holder for this preprint (which was not certified by peer review) is the author/funder, who has granted bioRxiv a license to display the preprint in perpetuity. It is made available under aCC-BY-ND 4.0 International license.

promoter. *Molecular Cell* 16: 725-736

Stark GR, Taylor WR (2006) Control of the G2/M transition. *Molecular Biotechnology* 32: 227-248

Stopak K, de Noronha C, Yonemoto W, Greene WC (2003) HIV-1 Vif blocks the antiviral activity of APOBEC3G by impairing both its translation and intracellular stability. *Molecular cell* 12: 591-601

Suzuki A, Badger BL, Salmon ED (2015) A quantitative description of Ndc80 complex linkage to human kinetochores. *Nature communications* 6: 8161

Swanstrom R, Coffin J (2012) HIV-1 Pathogenesis: The Virus. *Cold Spring Harbor Perspectives in Medicine* 2: a007443-a007443

Taylor WR, Stark GR (2001) Regulation of the G2/M transition by p53. *Oncogene* 20: 1803-1815

Vallardi G, Cordeiro MH, Saurin AT (2017) A Kinase-Phosphatase Network that Regulates Kinetochore-Microtubule Attachments and the SAC. *Prog Mol Subcell Biol* 56: 457-484

Vidya Vijayan KK, Karthigeyan KP, Tripathi SP, Hanna LE (2017) Pathophysiology of CD4+ T-Cell Depletion in HIV-1 and HIV-2 Infections. *Front Immunol* 8: 580

Wandke C, Barisic M, Sigl R, Rauch V, Wolf F, Amaro AC, Tan CH, Pereira AJ, Kutay U, Maiato H *et al* (2012) Human chromokinesins promote chromosome congression and spindle microtubule dynamics during mitosis. *Journal of Cell Biology* 198: 847-863

Wang J, Reuschel EL, Shackelford JM, Jeang L, Shivers DK, Diehl JA, Yu X-F, Finkel TH (2011) HIV-1 Vif promotes the G1- to S-phase cell-cycle transition. *Blood* 117: 1260-1269

Wang J, Shackelford JM, Selliah N, Shivers DK, O'Neill E, Garcia JV, Muthumani K, Weiner D, Yu X-F, Gabuzda D *et al* (2008) The HIV-1 Vif Protein Mediates Degradation of Vpr and Reduces Vpr-Induced Cell Cycle Arrest. *DNA and Cell Biology* 27: 267-277

Yu X, Yu Y, Liu B, Luo K, Kong W, Mao P, Yu X-F (2003) Induction of APOBEC3G Ubiquitination and Degradation by an HIV-1 Vif-Cul5-SCF Complex. *Science* 302: 1056-1060

Zhang P, Zhang Y, Gao K, Wang Y, Jin X, Wei Y, Saiyin H, Wang D, Peng J, Ma J *et al* (2015) ASPP1/2-PP1 complexes are required for chromosome segregation and kinetochore-microtubule attachments. *Oncotarget* 6: 41550-41565

Zhao K, Du J, Rui Y, Zheng W, Kang J, Hou J, Wang K, Zhang W, Simon VA, Yu X-F (2015) Evolutionarily conserved pressure for the existence of distinct G2/M cell cycle arrest and A3H inactivation functions in HIV-1 Vif. *Cell cycle* 14: 838-847

bioRxiv preprint doi: https://doi.org/10.1101/2024.07.30.605839; this version posted November 25, 2024. The copyright holder for this preprint (which was not certified by peer review) is the author/funder, who has granted bioRxiv a license to display the preprint in perpetuity. It is made available under aCC-BY-ND 4.0 International license.

693 **Figure Legends**

694 **Figure 1: Vif and Vpr induce distinct forms of mitotic arrest.**

695 (A) Representative live cell image for Cal51 cells with H2B-mScarlet and Tubulin-mNeonGreen
696 expressing Control, Vif, Vpr, or Vif+Vpr reporter viruses. (B) Average mitotic duration of Cal51
697 cells expressing respective reporter virus (n=100 for each from two replicates). (C) Frequency
698 of cell fate after mitosis for Cal51 cells expressing respective reporter virus. (n=100 for each
699 from two replicates)

700

701 **Figure 2: Vif induces robust pseudo-metaphase arrest.**

702 (A) Representative live cell images for Cal51 cells with H2B-mScarlet and Tubulin-mNeonGreen
703 expressing Control reporter virus. (B) Representative live cell image for Cal51 cells expressing
704 Vif reporter virus. (C) Frequency of cells that achieve metaphase plate and time taken to achieve
705 metaphase plate for cells in (A) and (B) (n=100 for each from two replicates). (D) Representative
706 live-cell images of Vif conditional expressed HeLa cell with or without Doxycycline. (E) Average
707 mitotic duration in condition (D) (n=100 cells for each from two replicates). (F) Quantification of
708 viable cells over time after Dox induction. (G) Quantification of apoptotic cells after Dox induction.

709

710 **Figure 3: Vif does not alter G1 or S phase progression, accelerates G2 progression, and**

bioRxiv preprint doi: https://doi.org/10.1101/2024.07.30.605839; this version posted November 25, 2024. The copyright holder for this preprint (which was not certified by peer review) is the author/funder, who has granted bioRxiv a license to display the preprint in perpetuity. It is made available under aCC-BY-ND 4.0 International license.

induces pseudo-metaphase arrest independent of p53

(A) Top: Representative image of Cal51 cells progressing through G1, S, and G2. Bottom: Representative trace for relative signal intensity of the nucleus through cell cycle. (B) Average duration of G1, S, and G2 phases in Control and Vif-expressing cells (n= 9 for Control and 11 for Vif, from two replicates). (C) Total cell cycle duration for Control and Vif-expressing cells. (D) Representative live cell images for Control and Vif-expressing WT or p35KO RPE1 cells. (E) Average mitotic duration in WT or p53KO RPE1 cells (n= >85 cells, from two replicates). (F) Frequency of cells which achieve metaphase plate for cells in (E). (G) Average time taken to achieve metaphase plate for cells in (F).

Figure 4: Vif induces polar chromosomes, multi-polar spindles, and abnormal chromosome movements

(A) Representative immunofluorescence images labeled for CENP-C (as a kinetochore marker), microtubule, and DNA in Control and Vif-expressing HeLa cells. (B) Example super-resolution images labeled for CENP-C, microtubule, and DNA in Vif-expressed HeLa cells showing polar chromosomes. (C) Representative live cell image of Vif-expressing cells where polar chromosomes were quantified by compartmentalizing polar regions. Bottom: Quantification of polar chromosome frequency overtime. (D) Representative high-temporal live cell images (6

bioRxiv preprint doi: https://doi.org/10.1101/2024.07.30.605839; this version posted November 25, 2024. The copyright holder for this preprint (which was not certified by peer review) is the author/funder, who has granted bioRxiv a license to display the preprint in perpetuity. It is made available under aCC-BY-ND 4.0 International license.

729 minutes interval) showing rapid chromosome moving towards and away from the spindle poles.
730 (E) Fraction of Cal51 cells showing abnormal number of poles at some point during mitosis. (F)
731 Top: Representative images of maximum mitotic spindle length for Control and Vif-expressing
732 Cal51 cells. Bottom: Average maximum mitotic spindle length of Control and Vif-expressing cells.
733 (G) Top: Representative live cell image of Control and Vif-expressing Cal51 cells over time
734 showing dynamic spindle spinning. Center: Representative figures showing relative orientation
735 (angle) of the spindle axis over time (radius). Bottom: Average total angle swept during mitosis.
736
737 **Figure 5: Vif, but not Vpr, disrupts the proper localization of PP2A-B56 at the kinetochores**
738 (A) Representative maximum intensity projection of fixed Control and Vif-expressing HeLa cells
739 with or without nocodazole treatment, immunofluorescently labeled for B56, CENP-C, and DNA.
740 (B) Representative maximum intensity projection of fixed Control and Vpr-expressing HeLa cells,
741 immunofluorescently labeled for B56, CENP-C, and DNA. (C) Average B56 level at kinetochores
742 for cells in (A) and (B) (n=200 kinetochores over 8 cells from two independent replicates for
743 each). (D) Representative fixed-cell immunofluorescent image of HeLa cells expressing Vif,
744 immunofluorescently labeled for Plk1, CENP-C, and DNA. (E) Average Plk1 level at kinetochores
745 for cells in (D) (n=200 kinetochores over 8 cells from two independent replicates for each).
746

bioRxiv preprint doi: https://doi.org/10.1101/2024.07.30.605839; this version posted November 25, 2024. The copyright holder for this preprint (which was not certified by peer review) is the author/funder, who has granted bioRxiv a license to display the preprint in perpetuity. It is made available under aCC-BY-ND 4.0 International license.

747 **Figure 6: Vif impairs stable and balanced kinetochore microtubule attachments**

748 (A) Left: Representative maximum intensity projection of fixed Control and Vif-expressing HeLa
749 cells immunofluorescently labeled for CENP-C, Astrin, and DNA along with representative sister
750 kinetochore pairs, Right: Illustrative interpretation of images on the left. (B) Average Astrin and
751 CENP-C level at kinetochores for cells in (A) (n = 200 kinetochores from 8 cells from two
752 independent replicates for each) (C) Comparison of Astrin and CENP-C on sister kinetochores,
753 values normalized with formula: 1 – (lower intensity value/higher intensity value). (D)
754 Representative image of fixed Control and Vif-expressing HeLa cells immunofluorescently
755 labeled for CENP-C, pHec1(S55), and DNA along with representative sister kinetochore pairs.
756 (E) Average pHec1(S55) level at kinetochores for cells in (D). (n = 200 kinetochores from 8 cells
757 from two independent replicates for each). (F) Comparison of pHec1(S55) on sister kinetochores,
758 values normalized with formula: 1 – (lower intensity value/higher intensity value). (G)
759 Representative fixed-cell immunofluorescent image of HeLa cells expressing Vif,
760 immunofluorescently labeled for Hec1, CENP-C, and DNA. (H) Average Hec1 level at
761 kinetochores for cells in (G) (n=200 kinetochores over 8 cells from two independent replicates
762 for each).

763

764 **Figure 7: Proposed model for the molecular mechanism underlying Vif's pseudo-**

bioRxiv preprint doi: https://doi.org/10.1101/2024.07.30.605839; this version posted November 25, 2024. The copyright holder for this preprint (which was not certified by peer review) is the author/funder, who has granted bioRxiv a license to display the preprint in perpetuity. It is made available under aCC-BY-ND 4.0 International license.

765 **metaphase arrest**

766 Top: Cartoon model depicting metaphase alignment of Control cells followed by anaphase.
767 Middle: Cartoon model depicting pseudo-metaphase alignment of Vif-expressing cells with
768 unbalanced microtubule attachment followed by three-step polar chromosome cycle. Bottom:
769 Cartoon depiction of three-step polar chromosome cycle, (1) chromosome at the equator is
770 pulled towards pole due to unbalanced pulling force, (2) kinetochore-microtubule destabilization
771 at the spindle pole, (3) equator-directed movement of chromosome for realignment.

bioRxiv preprint doi: https://doi.org/10.1101/2024.07.30.605839; this version posted November 25, 2024. The copyright holder for this preprint
CC BY-ND 4.0 International license

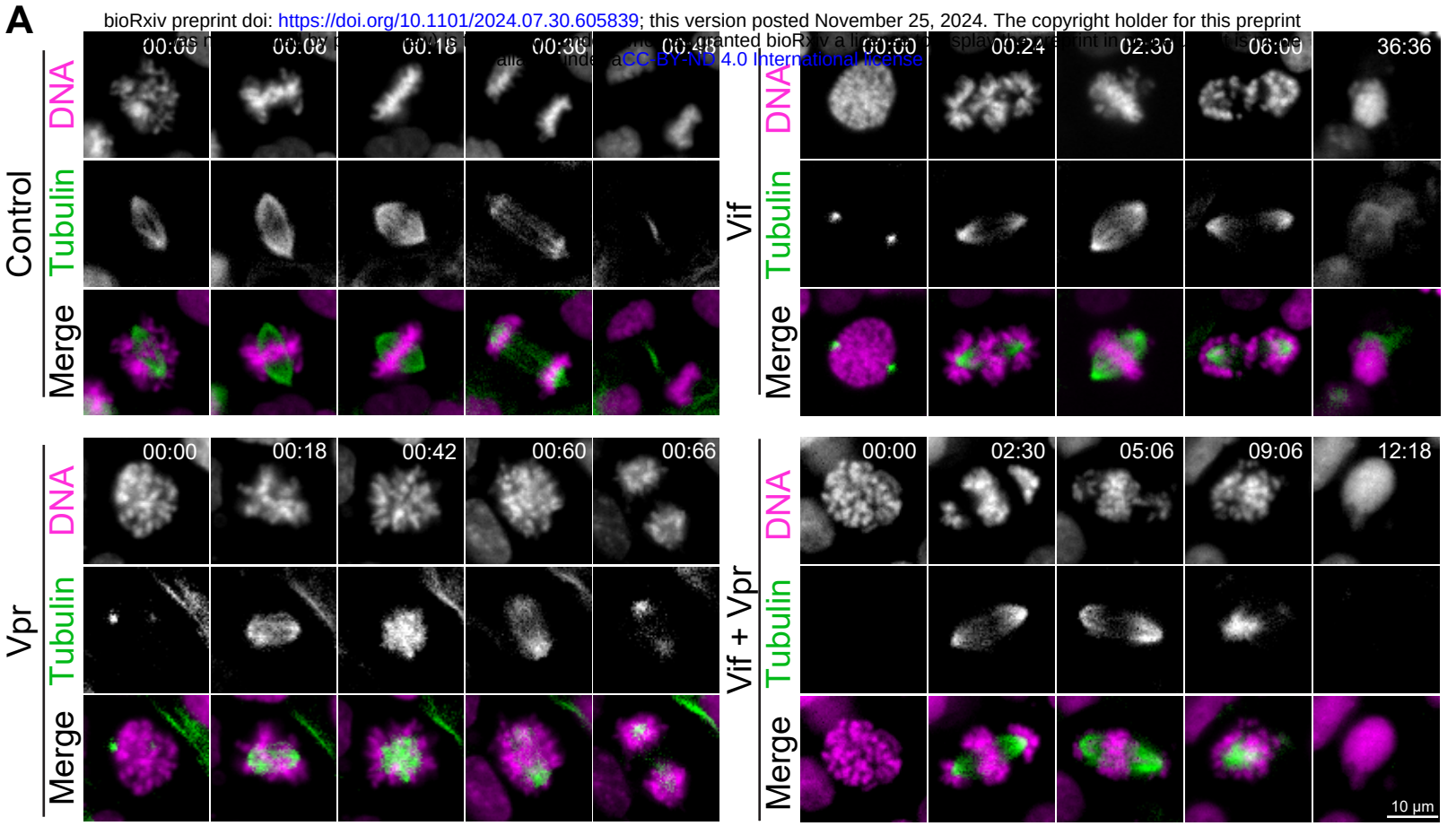

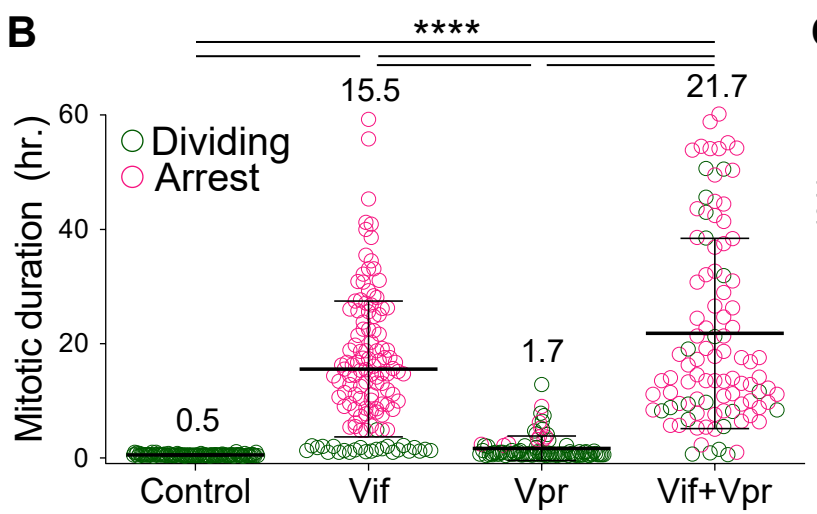

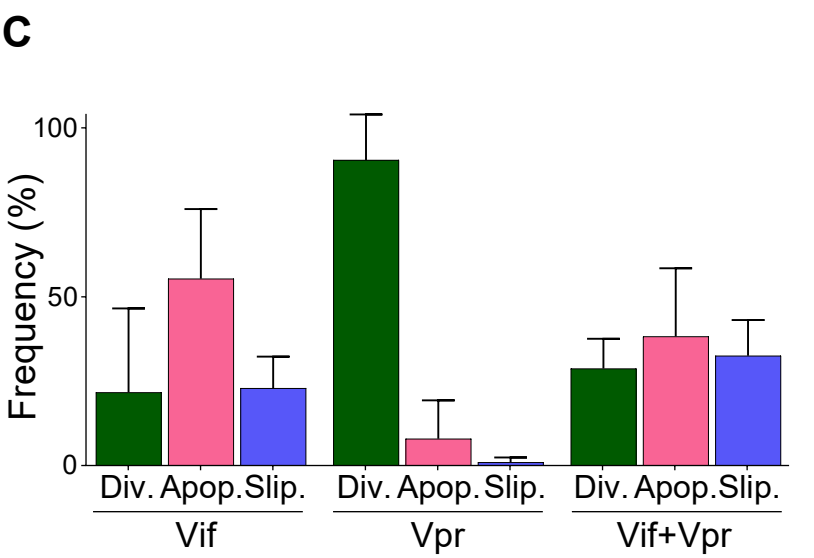

Figure 1

CC-BY-ND 4.0 International license

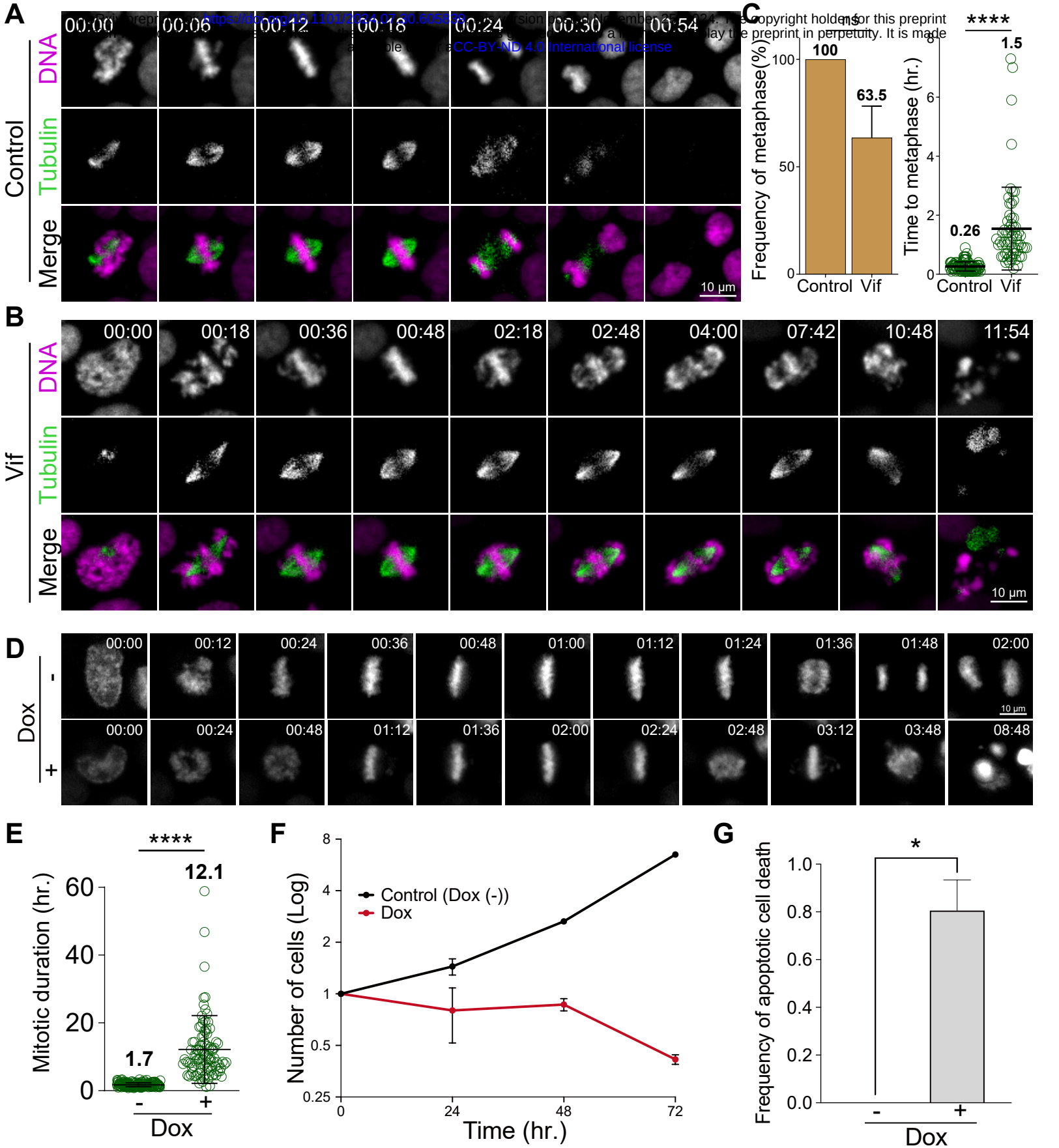

Figure 2

https://doi.org/10.1101/2024.07.30.605839
CC-BY-ND 4.0 International license

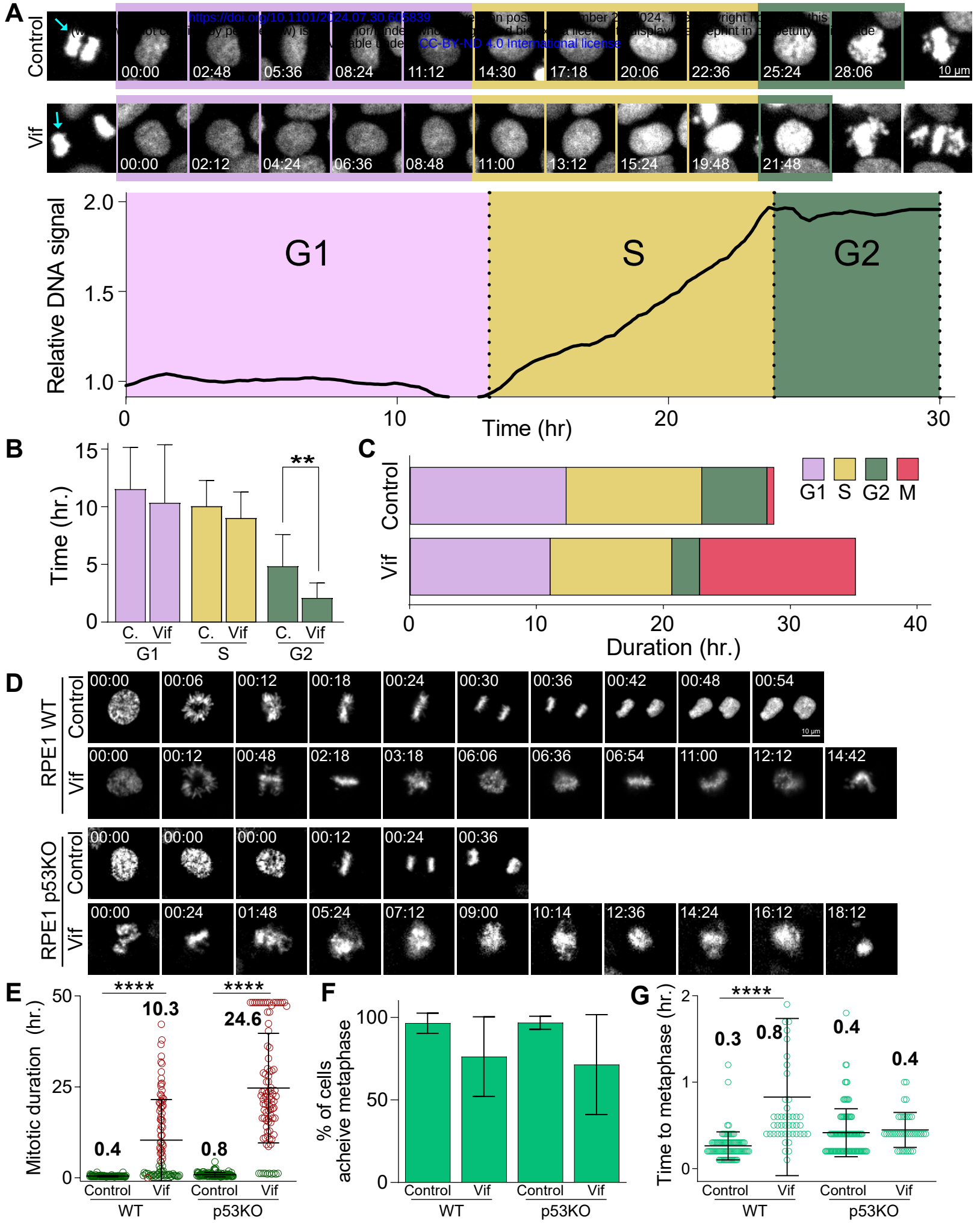

Figure 3

bioRxiv preprint doi: https://doi.org/10.1101/2024.07.30.605839; this version posted November 6, 2024. The copyright holder for this preprint (which was not certified by peer review) is the author/funder, who has granted bioRxiv a license to display the preprint in perpetuity. It is made available under aCC-BY-ND 4.0 International license.

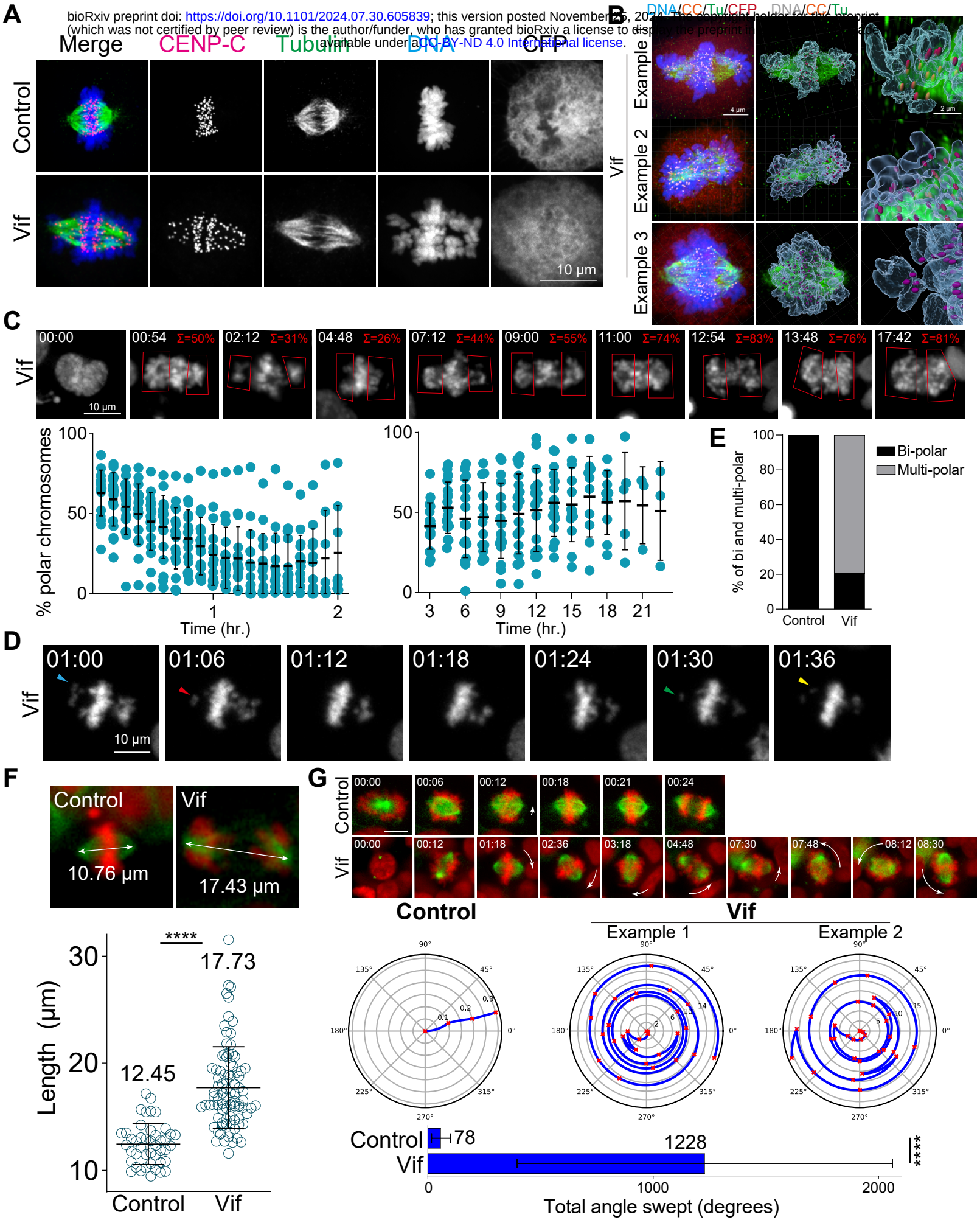

Figure 4

bioRxiv preprint doi: https://doi.org/10.1101/2024.07.30.605839; this version posted November 25, 2024. The copyright holder for this preprint (which was not certified by peer review) is the author/funder, who has granted bioRxiv a license to display the preprint in perpetuity. It is made available under a CC-BY-ND 4.0 International license

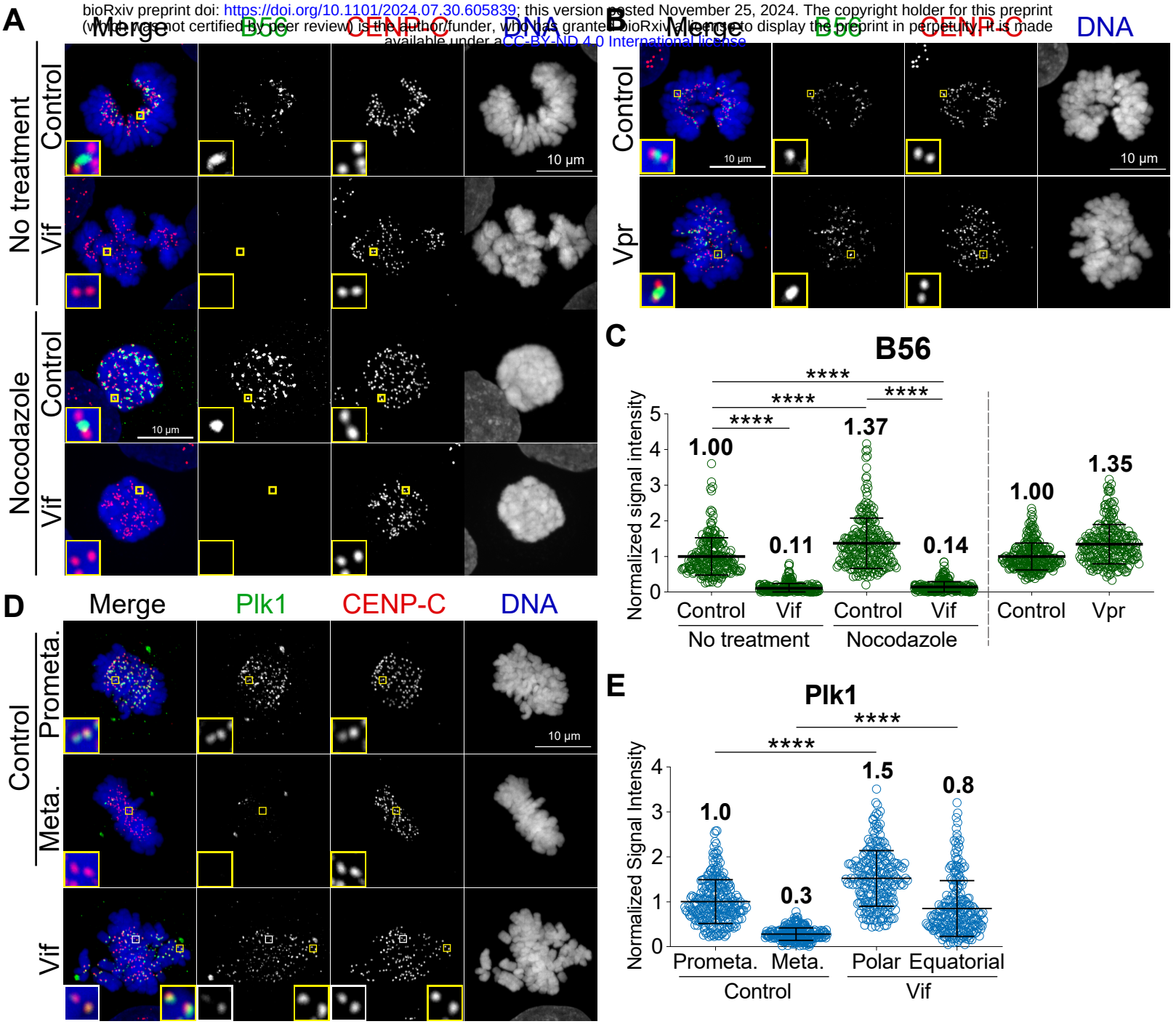

Figure 5

bioRxiv preprint doi: https://doi.org/10.1101/2024.07.30.605839; this version posted November 25, 2024. The copyright holder for this preprint (which was not certified by peer review) is the author/funder, who has granted bioRxiv a license to display the preprint in perpetuity. It is made available under aCC-BY-ND 4.0 International license.

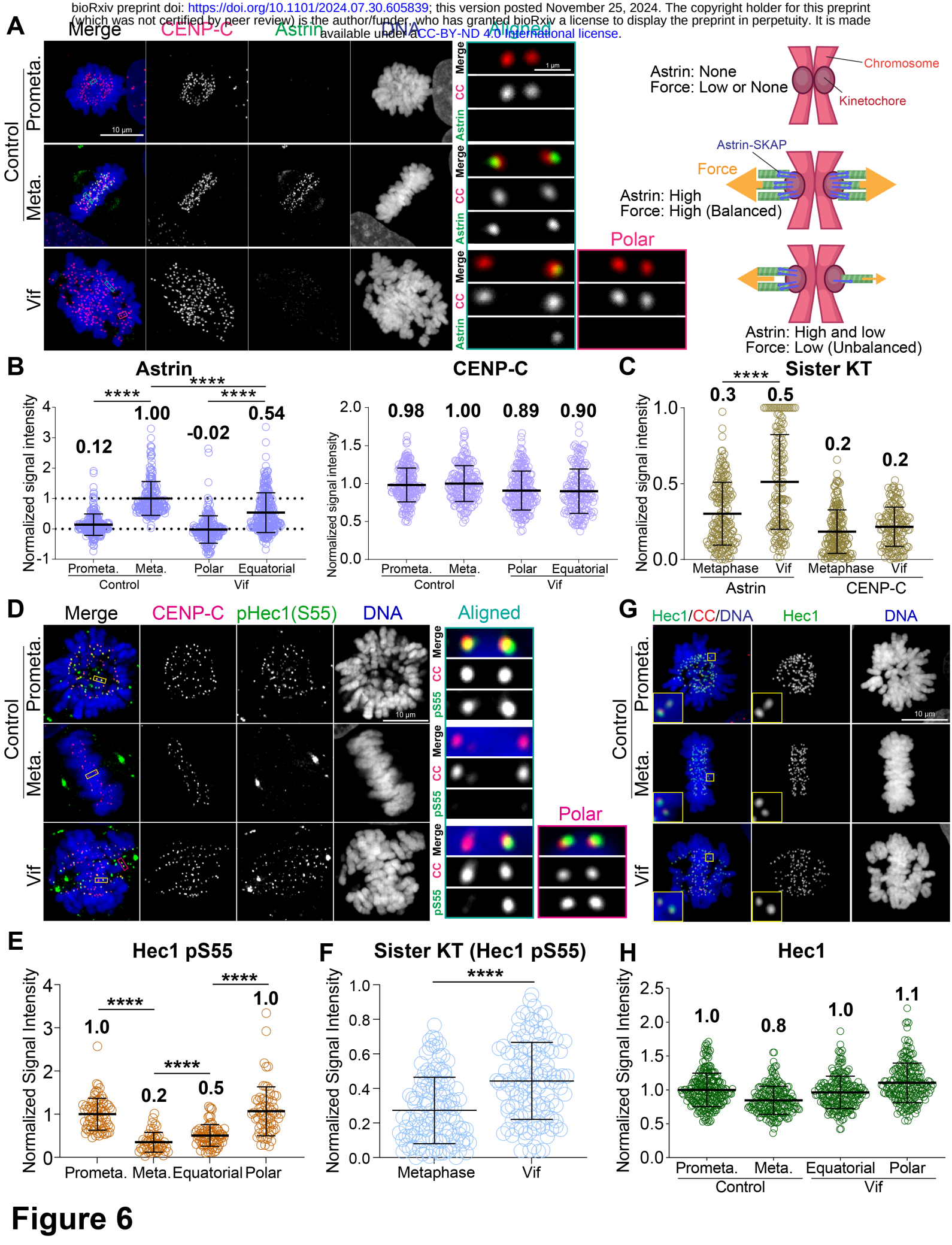

Figure 6

bioRxiv preprint doi: https://doi.org/10.1101/2024.07.30.605839; this version posted November 25, 2024. The copyright holder for this preprint (which was not certified by peer review) is the author/funder, who has granted bioRxiv a license to display the preprint in perpetuity. It is made available under aCC-BY-ND 4.0 International license.

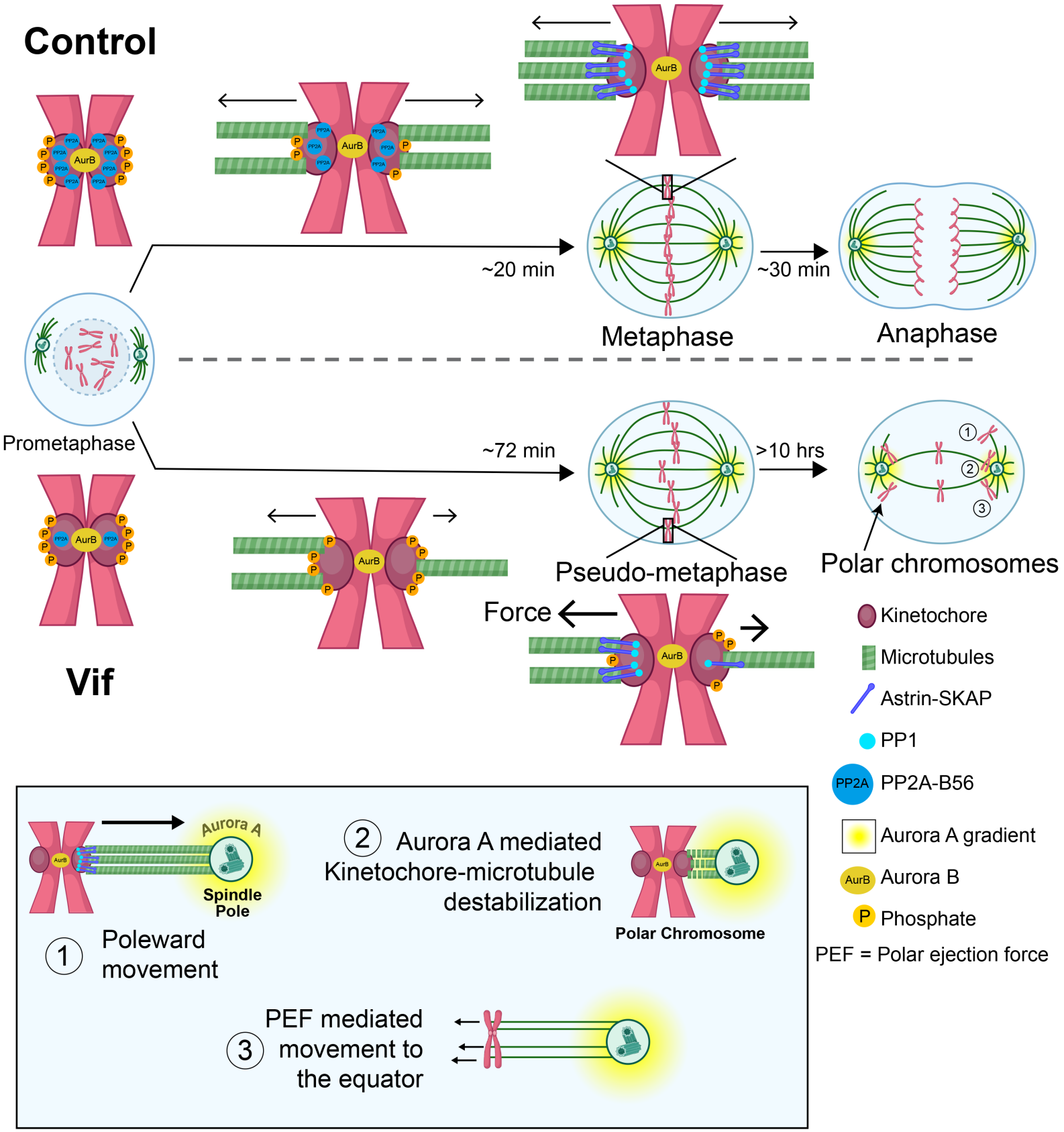

Figure 7